UNIVERSITY OF TARTU

FACULTY OF SCIENCE AND TECHNOLOGY

Institute of Technology

and

CHALMERS UNIVERSITY OF TECHNOLOGY

DEPARTMENT OF CHEMISTRY AND CHEMICAL ENGINEERING

Silver Jõemetsa

RAPID PROTOTYPING AND CHARACTERIZATION OF LIPID MEMBRANES ON SOLID SURFACES

Master's thesis

Supervisors:

Dr. Alar Ainla

Associate Professor Aldo Jesorka

Professor Alvo Aabloo

Tartu 2015

Table of Contents

Abbreviations

CLSM	confocal laser scanning microscopy
DOPE	1,2-dioleoyl-*sn*-glycero-3-phosphoethanolamine
DOPS	1,2-dioleoyl-*sn*-glycero-3-phospho-L-serine
DOTAP	1,2-dioleoyl-3-trimethyl-ammoniumpropane
FC-40	perfluorotri-n-butylamine mixture with perfluoro-n-dibutylmethylamine
FC-75	perfluoro(2-butyl tetrahydrofuran)
FRAP	fluorescence recovery after photobleaching
HCF	hydrodynamically confined flow
LIF	laser-induced fluorescence
MFP	Multifunctional Micropipette
PBS	phosphate buffered saline
PDMS	poly-(dimethylsiloxane)
PMT	photon multiplier tube
POPC	1-palmitoyl-2-oleoyl-*sn*-glycero-3-phosphocholine
Soy PC	Soy L-α-phosphatidylcholine
SUV	small unilamellar vesicle
Teflon-AF	poly[4,5-difluoro-2,2-bis(trifluoromethyl)-1,3-dioxole-co-tetrafluoroethylene]
TRIS	2-amino-2-hydroxymethyl-propane-1,3-diol

1 Introduction

The living nature is an elaborate contraption, consisting of different types of organized structures and a vast variety of materials. The most important autonomous unit of living organisms, which has all the required attributes of life, is a biological cell. The cell is surrounded by the plasma membrane, which is one of the most important self-assembling structures in the biological world. The plasma membrane is a planar molecular bilayer consisting mainly of phospholipids. The cell membrane has several crucial functional and structural properties: it acts as a protective vessel for cell organelles separating intracellular and extracellular environments, it is also a selectively permeable gateway, facilitating numerous transport modes (diffusion, endo- and exocytosis) concurrently incorporating transmembrane proteins, which act as channels and pumps to allow the transport of nutrients into and waste product out of the cell. The cell membrane and its constituents also allow the cell to communicate with its surrounding. This membrane is very dynamic – it can restructure and change its shape, and it constitutes the two-dimensional medium hosting various molecules, such as steroids, proteins and others, that facilitate many of these intricate behaviors[1]. Despite the abundant research on lipids in the membrane and their various complex functions, the whole picture is still far from complete.

The need to understand the properties of cell membranes and the fundamental mechanisms of molecular interactions has stimulated researchers to build simplified 2D models[2,3]. A popular class of 2D model systems is a supported membrane. Several nanometers thick bilayers[4] and monolayers[5,6] or multi-bilayer membranes can be formed on solid supports, depending on the preparation technique, the hydrophobicity of the surface, the lipid head-group properties and the ionic strength of the surrounding solution[7,8]. These solid-supported membranes are excellent models to study the features of the cell membranes at reduced complexity, especially due to the possibility of using a wide variety of powerful surface-specific analytical techniques (*e.g.* atomic force microscopy, quartz crystal microbalance, surface plasmon resonance etc.) and microscopy (*e.g.* TIRF, confocal). While most of the current research is focused on lipid bilayer architectures on solid supports, there is a growing interest in monolayer film fabrication and use, primarily motivated by their biological importance. Examples are found in the pulmonary system, where a monolayer lipid film lowers the surface tension of the alveoli, assisting the inflation of the lungs[9,10] whereas monolayer lipids in the tear film of the eye protect it from drying[11,12].

Recently, a new open volume approach was developed[13] that is fundamentally different from the other miniaturized technologies currently used to assemble artificial bilayer systems[14]. It is a microfluidic toolbox to write 2D nanofluidic networks composed of supported phospholipid membranes, and dynamically modify their connectivity, composition, and local function[15] using a multifunctional pipette (MFP). It is called the "lab on a biomembrane" (LoaBM) technique.

The main objective of this research is to advance the LoaBM technique and increase the number of available support materials. This is achieved by performing a systematic study with the MFP to examine the effect of the lipid composition and support properties on lipid spreading and deposition. Eight different high- and low-energy surfaces (Au, borosilicate glass, quartz, Si_3N_4, SiC, SU-8, graphene and Teflon-AF) have been investigated, while the lipid suspensions consisted of 9 different concentrations of the cationic and anionic lipids: DOTAP, POPC, Soy PC and DOPS together with a small fraction of lipids linked with flourophores. These experiments would further demonstrate the simplicity, flexibility and reproducibility of the LoaBM technique for prototyping molecular lipid films in various conditions, which in turn would lead to a powerful toolbox to study the properties and interactions of the cell membrane and its components. It would both lead to a better understanding of the fundamental mechanisms in membrane biophysics (e.g. cell signaling) as well as enable potential uses for biomedicine, pharmacology etc. For example, it has been shown that controlled drug-delivery can be achieved by modifying the compositions of lipid nanocontainers[16].

2 Background

2.1 Surfaces

2.1.1 Surface properties

In order to understand the propagation of lipid molecules on solid surfaces one needs to know the properties of the surfaces in question. While some of the properties are intuitively understandable such as, molecular composition, geometry, others are still more difficult to comprehend. Therefore the concepts of surface energy, surface tension, contact angles, roughness and surface charge, which are all characteristic to surfaces, will be described.

The atoms at the surface of a solid material always have a higher potential energy in comparison to the atoms in the bulk, because of fewer neighbors on the surface than in the bulk (Figure 1). It can also be said that the cohesive interactions between molecules in the bulk are more favorable than at the surface. As all systems strive to minimize their free energy, solid materials tend to decrease their energy by forming new bonds with molecules in their vicinity *i.e.* the first coordination sphere. The difference between the energy of molecules on the surface and in the bulk is called the *surface free energy* (F), which is a measure of showing how much energy that surface has per unit area.

The *surface tension* of a material (γ) is determined by the surface free energy and is represented as the tangential stress (force per unit length) in the surface layer [17].

$$\gamma = F + A\frac{\partial F}{\partial A}, \qquad 2.1.1$$

where A is the area of the surface. The term $\partial F/\partial A$ describes the induced volume stress in a solid after deformation of the volume *e.g.* the solid is compressed while splitting a block of the material into two pieces. Solid materials cannot balance this stress as their atoms are immobile and after any deformation their relative positions are preserved, whereas molecules in a one-component liquid are transferred between the surface and the interior during deformation, which balances the extra energy. This rearrangement will lead to $\partial F/\partial A = 0$, thus $\gamma = F$ in a liquid.

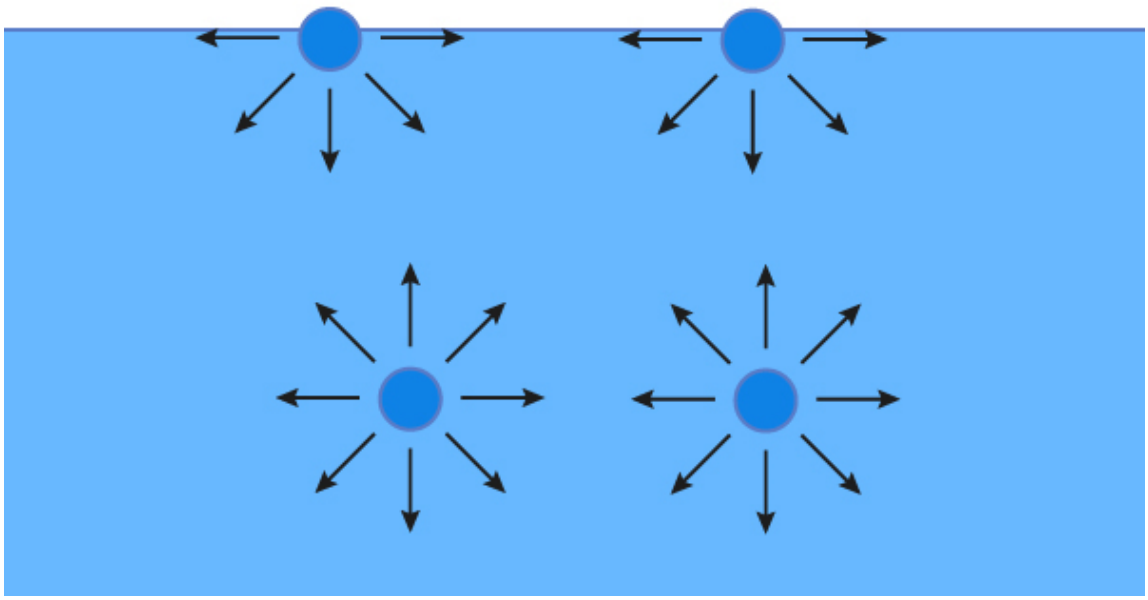

Figure 1. The molecules on the surface experience less cohesive interactions compared to molecules in the bulk.

The surface component of the free energy of colloidal systems is described with the following equation:

$$G_{surface} = \sum_i \gamma_i A_i \qquad 2.1.2$$

Colloidal systems can reduce this free energy either by reducing surface and interface areas A_i or by reducing the system's surface tensions γ_i by adsorbing surfactants. It should be noted that the surface component of the free energy $G_{surface} = 0$ for large scale chemical systems.

As already elaborated previously, molecules at the surface tend to minimize their free energy *i.e.* increase their coordination with neighboring molecules, which is also the reason why chemical adsorption of water and the formation of OH^- groups occur on newly synthesized oxides. The *surface charge* on oxides results from the ionization of the previously formed hydroxyl groups on the surface upon contact with water. This equilibrium of a metal (M) oxide and water can be depicted as [18] :

$$M - O^- + H_3O^+ \rightleftarrows M - OH + H_2O \rightleftarrows M - OH_2^+ + HO^-$$

The charge on a surface can be negative, positive or zero, depending on the nature of the oxide in question and the pH of the surrounding buffer.

Other dominating means to reduce the surface energy of a substrate are through the formation of van der Waals and hydrogen bonds on the liquid interface [19]. The latter is known as *surface wetting* and refers to the tendency of a liquid to spread on a solid surface. As different materials have different tendencies to be wetted by liquids, they are divided into high-energy and low-energy surfaces. High energy surfaces are metals, oxides, nitrides with strong covalent, ionic or metallic bonds *i.e.* strong cohesive forces between their atoms, whereas low-energy surfaces are often polymers with covalently bonded chains that are held together by weak intermolecular van der Waals forces.

The hydroxyl groups, among others, contribute significantly to wettability on solid surfaces[20,21].

It is common to categorize surfaces based on their interactions with water only. They can be hydrophilic (polar) *i.e.* water-friendly or hydrophobic (non-polar) *i.e.* water-fearing. Therefore high-energy surfaces are generally hydrophilic, whereas low-energy surfaces are hydrophobic.

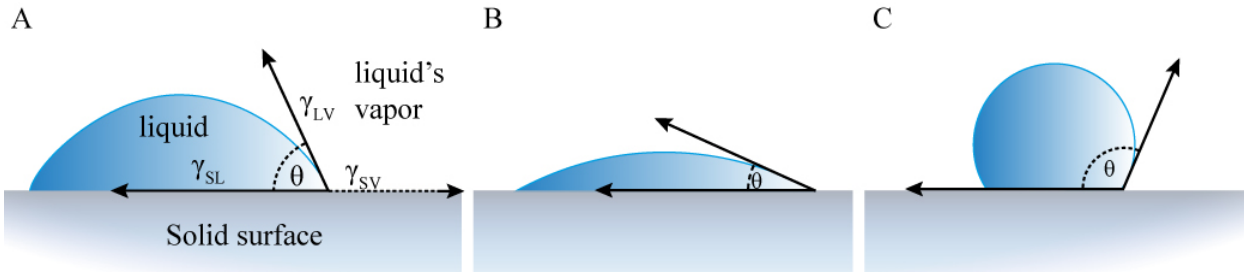

Figure 2 (A) Illustration of the contact angle θ and interfacial tensions of a water droplet wetting a solid surface. (B-C) A water droplet on a (B) hydrophilic surface, $\theta < 90°$ (C) hydrophobic surface, $\theta > 90°$.

Wetting is usually described by the contact angle θ of a droplet on a surface. At the contact line, where the droplet touches the solid surface the interfacial tensions, solid-vapor (γ_{SV}), solid-liquid (γ_{SL}) and liquid-vapor (γ_{LV}), are in a force balance, which is depicted in Figure 2. Young's equation expresses this thermodynamic equilibrium between the liquid (L), solid (S) and vapor (V) phase:

$$\gamma_{SV} - \gamma_{SL} = \gamma_{LV} \cos\theta \qquad 2.1.3$$

Hydrophilic surfaces have an equilibrium contact angle $\theta < 90°$, because the surface tension of the pure solid γ_{SV} is larger than the interfacial tension γ_{SL} between the droplet and the

surface. In short the spreading of the water droplet, in order to increase the contact area on the high-energy surface, is energetically favorable. In comparison, the contact angle between a hydrophobic surface and water $\theta > 90°$, which leads to more spherical shaped droplets on the corresponding solid surface. Nonetheless, the *roughness* of a surface can contribute to a significantly larger contact angle[22]. The natural water repellency of the lotus leaf and the water strider leg[23] are examples of rough surfaces, with extraordinarily high contact angles $\theta \geq 150°$, the so-called superhydrophobic surfaces[24,25]. The extreme roughness on those surfaces is created by microscale pillars and nanoscale surface irregularities on top of those pillars, which trap the air between the surface and the droplet and increase the liquid-vapor contact area[26]. These are cases of heterogeneous wetting and are described with the Cassie-Baxter model[24].

In order to explain different contact angles on identical materials with different levels of roughness, the Wenzel model is used[22,25], which describes the homogeneous wetting regime, where complete liquid penetration into the roughness grooves occurs:

$$\cos\tilde{\theta} = \frac{A_r}{A_0}\cos\theta\,, \qquad 2.1.4$$

where $A_r/A_0 = r$ is the roughness factor, which shows how much the drop's solid-liquid interface is enlarged by the real surface area A_r compared to the macroscopic surface area of the smooth case A_0, giving the contact angle on a rough surface $\tilde{\theta}$. The conditions for determining the transition between the two wetting regimes have been discussed by Marmur[27].

2.1.2 Examples of surfaces

As already described previously, supported lipid bilayers can be assembled on many high-energy surfaces, such as metals, metal oxides, semiconductor oxides and nitrides, with surface energies well above 100 mJ/m², while supported monolayers can be assembled on low-energy surfaces such as polymers and fiber composites, with surface energies typically less than about 50 mJ/m².

The most common surfaces used for lipid membrane adhesion are optically transparent materials, which are compatible with many microscopy and spectroscopy methods, for example fluorescence microscopy, which was used in this thesis.

In this research the high-energy surfaces used for lipid bilayer adhesion were gold, silicon nitride (Si_3N_4), quartz, borosilicate glass and silicon carbide (SiC), but others could also be used, such as the atomically smooth mica or soda-lime glass. In contrast, the low-energy surfaces used for monolayer adhesion were SU-8, graphene and Teflon AF®.

Most of these surfaces *i.e.* Si_3N_4, Au, SU-8 and Teflon AF, have been deposited onto solid glass or silicon substrates in thin transparent layers via different methods explained in the following chapter.

These transparent substrates need to be cleaned very thoroughly to remove all contaminants in order to avoid the contamination of the film that is being deposited and guarantee the best adhesion with the substrate. High-energy substrates *e.g.* borosilicate glass are easily contaminated by tiny amounts of oils, greases and other relatively low-energy materials, which cover the substrate in thin layers. Therefore a common pretreatment is washing the surface with solvents in combination with an ultrasonic bath. The most effective is wet cleaning with piranha.

2.1.3 Surface processing techniques

The surfaces required for the lipid spreading experiments were fabricated in the Nanofabrication Laboratory MC2 at Chalmers, a state-of-the-art cleanroom for the processing of materials required in micro- and nanoelectronics.

A wide range of techniques exists to deposit thin films *e.g.* atomic layer deposition, chemical vapor deposition, reactive sputtering etc., while the ones used in this research will be explained briefly.

2.1.3.1 Spin-coating

Spin-coating is a well-known and straightforward method introduced more than 50 years ago[28], which involves the deposition of a droplet on a substrate and then spinning the substrate at high speeds in order to spread the liquid material into a uniformly thin-film by centrifugal force. It is most extensively used in the microelectronics industry for photoresist coatings, which typically have film thicknesses in the micro- and nanometer range.

The final thickness of the film and other properties will depend on the nature of the solution and the solvent (viscosity, evaporation rate, surface tension, etc.) and the parameters chosen

for the spin process. Factors such as final rotation speed, acceleration, and fume exhaust affect the properties of the coated films. In general, the higher the angular speed of spinning, the thinner the film.

2.1.3.2 Sputter deposition

Sputtering is a method of thin-film deposition of various materials in a chamber filled with a rarified inert gas, which is ionized and used to bombard the target material with ions. The material removed from the target is deposited on the sample surface.

In direct current (DC) sputtering a high potential difference between the target material (cathode), and the substrate (anode) is applied. The electrons emitted from the cathode are accelerated towards the anode and collide with the inert gas (usually argon) atoms, which are ionized by the impact of electrons. These argon ions are accelerated towards the negatively charged target surface and with high enough energies (10-5000 eV) the surface atoms will be ejected from the target (sputtering process). These atoms, and atomic clusters cross the evacuated chamber and condensate as a thin-film at the opposing surface.

In Reactive Sputter Deposition, the deposited film is formed by the chemical reaction between the surface atoms of the target material (in our case silicon) and with the atoms of the ambient gas (N_2), which is introduced into the vacuum chamber.

In radio-frequency (RF) sputtering there is no DC between the anode and cathode, since the current alternates at high frequencies. It is mostly used to sputter insulators that require high bias for the sputtering process to occur. By using an alternating current, a build-up of charges at the target and at the substrate, which leads to the decrease in voltage, is prevented.

The Si_3N_4 surfaces used in the experiments were deposited with the RF sputtering method.

2.2 Phospholipid membranes

Lipids are amphiphilic molecules, which contain a hydrophilic (polar) head-group and a hydrophobic (non-polar) tail-group in their molecular structure. They are generally categorized as phosphoglycerides, sphingolipids and sterol lipids, based on the chemical nature of their backbone.

Phospholipids (phosphoglycerides) make up an important class of lipids, being the main constituents of biological cell membranes. The plasma membrane constitutes the two-dimensional medium in which molecules, such as proteins, steroids and others are solvated in. It also acts as a protective vessel for cell organelles separating the intracellular and extracellular spaces and is concurrently the mediator between the communication of cells and their surroundings. The membrane must be semi-permeable to allow the transport of nutrients into and waste product out of the cell.

The phospholipids are not "true fats" because they have one of the fatty acids replaced by a phosphate group. When fully hydrolyzed, phospholipids break down into smaller units: fatty acids, glycerol, a phosphate group, and the head-group, such as choline[29]. The phospholipid head group is linked to two hydrophobic hydrocarbon tails through a phosphate group and glycerol. In most biological membranes, hydrocarbon tails contain 10 to 18 carbons per chain. Carbons can be linked either by single bonds (saturated) or double bonds (unsaturated) and the chain may also include branching. The structure of a phospholipid molecule can be found on Figure 3.

There are other examples of amphiphilic molecules, such as proteins, copolymers and especially surfactants, such as sodium dodecyl sulfate (SDS), which all have the tendency to associate into numerous types of organized small assemblies and extended structures [30].

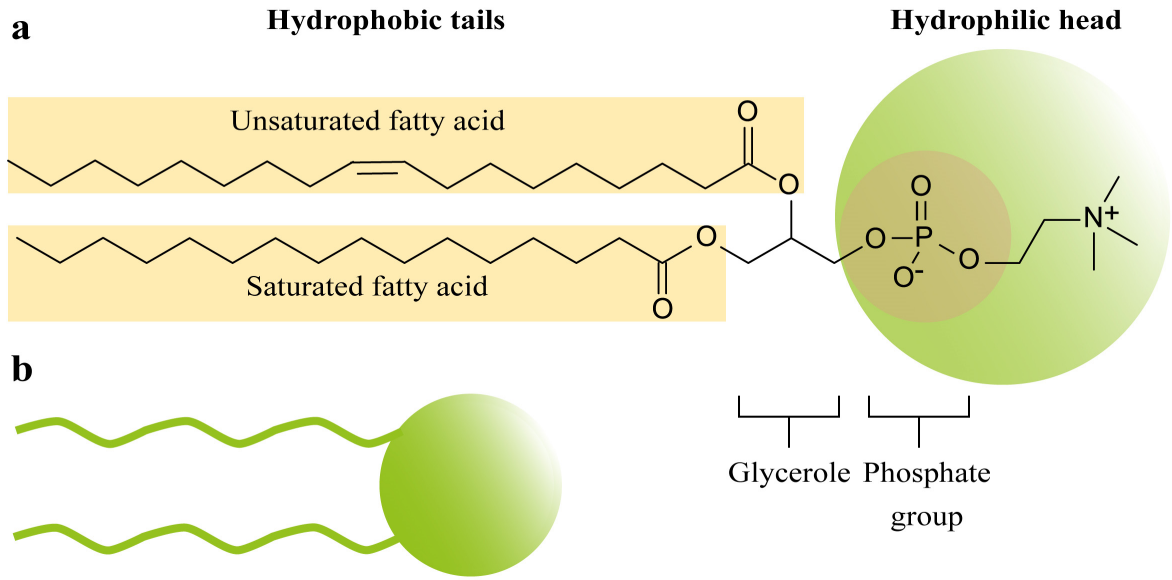

Figure 3 (a) An example of the phospholipid molecule POPC depicting the polar head-groups, non-polar tail-groups, fatty acid chain saturation and other structural units. (b) A simplified representation of a phospholipid.

When dissolved in an aqueous solution, the hydrophilic head of lipids screen the hydrophobic tails and spontaneously form aggregates in order to minimize the free energy, referred to as the "hydrophobic effect"[31]. The spontaneous organization process of lipids (and other amphiphiles) from a disordered state to an ordered arrangement is referred to as "self-assembly". The latter is a thermodynamically driven process. When water molecules come in contact with the non-polar part of a lipid molecule, H-bonds between water molecules are lost[32]. As water has a high tendency to form hydrogen bonds with other polar molecules, then in the liquid state, each water molecule participates in 3-3.5 H-bonds with its nearest neighbors[30]. If the molecule is small, water molecules salvage the lost H-bonds by wrapping around the molecule without terminating any bonding, known as "hydrophobic solvation". It should be noted that the interaction between a hydrophobic molecule and water is actually still attractive due to the dispersion force, but the interaction with other water molecules is just much more attractive[30].

However, the situation, where water molecules are exposed to a hydrophobic interface is thermodynamically highly unfavorable, because the newly formed rigid configurations have a high degree of order, which naturally corresponds to a decrease in entropy. The system will always tend to increase its entropy and minimize its free energy. Nevertheless, during spontaneous self-assembly the extra ordering imposed by the hydrophobic parts of lipid molecules is reduced if they are brought closer together, hence arranging away from the

exposure to water, which liberates the water molecules from the rigid configurations and restores hydrogen bonding. The change in the Gibbs free energy (ΔG) of the system is:

$$\Delta G = \Delta H - T\Delta S\,, \qquad 2.2.5$$

where ΔH is the change in enthalpy and $T\Delta S$ is the change in entropy, which shows the degree of order a system has before and after the self-assembly. It should also be noted that for a spontaneous process *i.e.* self-assembly, the change in free energy is $\Delta G < 0$. Even though lipid molecules are assembling into organized structures, the overall entropy is still increasing (due to water) and accordingly the free energy is reduced. As a result of this, lipid molecules spontaneously self-assemble into various organized structures hiding their hydrophobic tails.

The type of the organized structure is determined by the effective head-group area, critical chain-length and hydrocarbon volume of the lipids (Table 1)[33].

The critical packing parameter (CPP) shows which geometries can be formed depending on the shape of the amphiphile:

$$CPP = \frac{V}{AL}\,, \qquad 2.2.6$$

where V is the volume taken by the hydrophobic (tail) part, A is the effective surface area of the head-group and L is the length of the tail-group. Single-chained lipids (surfactants) with bulky head-groups *i.e.* $CPP < 0.5$, tend to form micelles, phospholipids with large head-group areas *i.e.* $0.5 < CPP < 1$ tend to form bilayes and vesicles, whereas lipids with large hydrophobic tails *i.e.* $CPP > 1$ prefer to form reverse crystal phases, such as inverted micelles[30]. As many phospholipids have a cylindrical shape *i.e.* CPP around 1, they tend to form vesicles, which are closed bilayers where part of the external aqueous medium is encapsulated inside the membrane. There are numerous parameters, which affect the CPP and consequently the geometry of the structure, such as electrolyte and lipid concentration, pH or temperature, as they will change the interactions between the lipid aggregates and also the intermolecular forces within each aggregate. For example the addition of electrolytes will partially screen the electrostatic repulsion between head-groups and will therefore reduce the effective surface area of the head-group.

Table 1 Critical packing shapes of lipids and the structures they form. This drawing is the adapted and simplified version of the original by Israelachvili.[30]

Lipid	Critical packing parameter (CPP)	Critical packing shape	Structures formed
Single-chained lipids (surfactants) with large head-group areas, *e.g.* SDS	< 1/3	Cone 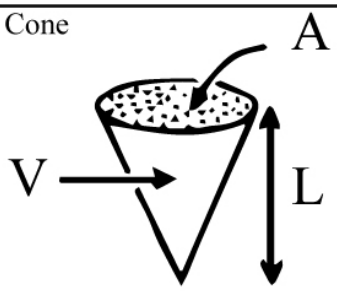	Micelles 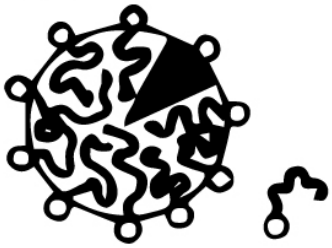
Double-chained lipids with large head-group areas, *e.g.* POPC	1/2 - 1	Truncated cone 	Flexible bilayers, vesicles 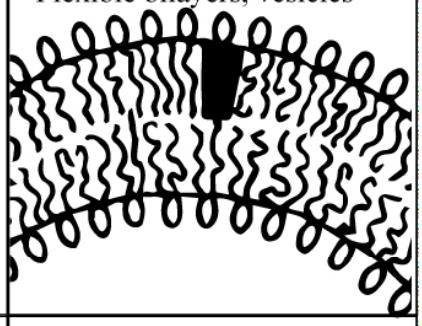
Double-chained lipids with small head-group areas, anionic lipids in high salt, *e.g.* DOPE	~1	Cylinder 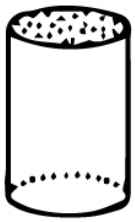	Planar bilayers 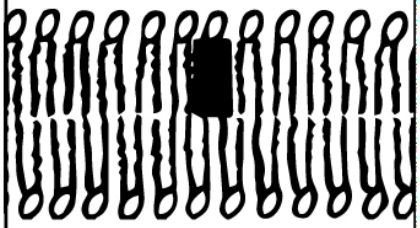
Double-chained lipids with small head-group areas, nonionic lipids, *e.g.* cholesterol	>1	Inverted truncated cone 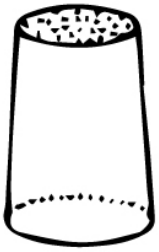	Inverted micelles 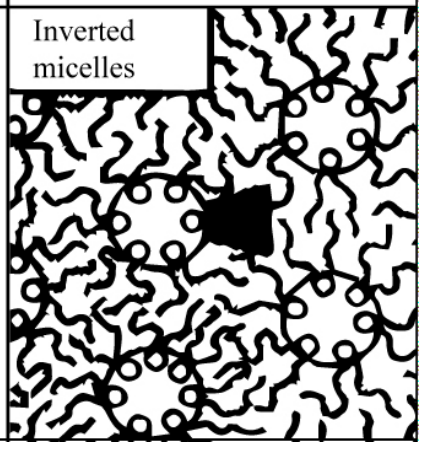

Vesicles are often classified according to their size and number of bilayers. If a vesicle consists of a single bilayer then it is called a unilamellar vesicle. Vesicles that have more than one bilayer are referred to as multilamellar (Figure 4). Based on their size they are classified as small (10-50 nm), large (50-1000 nm) and giant vesicles (larger than 1 μm). Only small unilamellar vesicles (SUVs) were used in this research to form lipid mono- and bilayers.

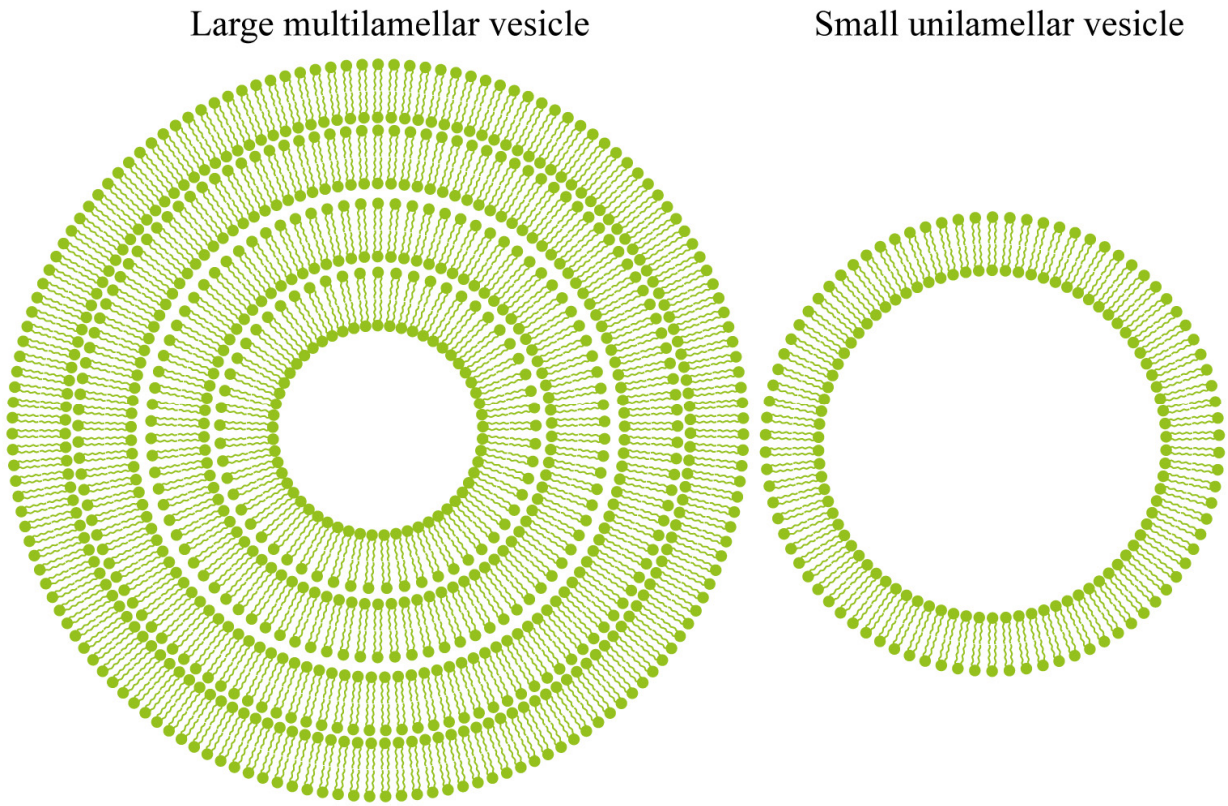

Figure 4 Examples of cross-sections of two common vesicle types.

2.3 Supported lipid membranes

Solid-supported membranes are excellent model systems to study the features of the plasma membranes of biological cells. The solid support provides greater stability for the lipid membrane and renders it possible to use a wide variety of powerful surface-specific analytical techniques (*e.g.* atomic force microscopy, quartz crystal microbalance, surface plasmon resonance etc.) [34] and microscopy. Depending on the preparation technique, the lipid head-group properties, the ionic strength of the surrounding solution and especially the hydrophobicity of the surface [7,8], it is possible to form on substrates bilayer[4] and monolayer[5,6] membranes, which are several nanometers thick. In general, if the surface is hydrophilic, a bilayer is formed, while hydrophobic surfaces lead to monolayer lipid films[5,35] (Figure 5).

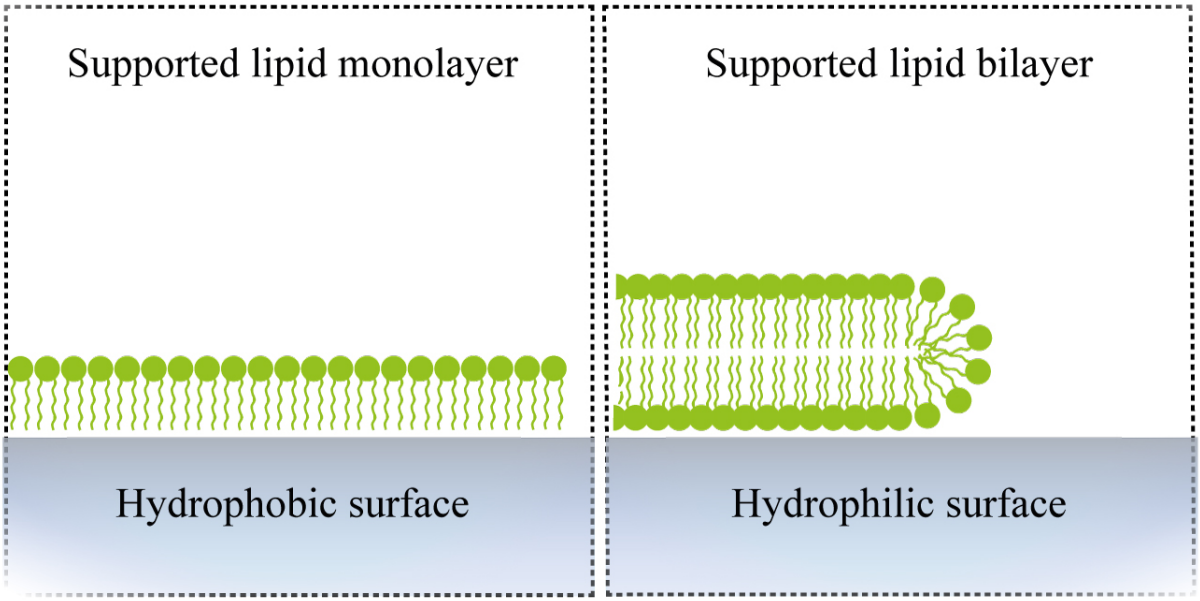

Figure 5. A supported lipid monolayer and a supported bilayer. It should be noted that the monolayer is directly in contact with the surface, whereas a water layer is trapped between the bilayer and the substrate.

2.3.1 Lipid bilayers

Lipid bilayers comprise of two physically very different environments. The hydrophobic bilayer interior is a relatively homogeneous region of hydrocarbon chains and the exterior comprises of the hydrophilic head-groups, which face towards the aqueous medium. The sheets of the bilayer are held together by hydrophobic interactions, the unusually strong attraction forces of hydrophobic molecules in water[30,36]. Solid supported lipid bilayers provide an excellent model system for studying the surface chemistry of the cell. For example, they retain two-dimensional fluidity and can be an excellent environment to incorporate membrane proteins. Lipid bilayers can be adsorbed on hydrophilic high-energy surfaces as mentioned

previously. In solid supported systems membrane fluidity is maintained by a 10–20 Å layer of trapped water between the substrate and the bilayer[37–39].

It is quite well known that on hydrophilic, negatively charged surfaces such as SiO_2 the adhesion of the membrane to the surface is facilitated by buffers with high ionic strength[40,41], in particular when multivalent ions such as calcium (Ca^{2+}) and magnesium (Mg^{2+}) are present, which screen the negative charges of negative head-group lipids and the surface or even act as cross-linkers between the lipids and the surface. Furthermore, even when the bulk concentration of Ca^{2+} is much smaller than that of Na^+ the surface may have a much higher local concentration of Ca^{2+}. On negatively charged surfaces such as SiO_2, divalent ions often bind chemically to negative surface sites (*e.g.* $Si\text{-}O^-$) and reduce the surface charge. It is not unusual for surfaces to be completely neutralized in the presence of mM amounts of Ca^{2+} [30].

In order to support a bilayer with little defects and high mobility, the surface should be hydrophilic, smooth and clean.

2.3.2 Lipid monolayers

In comparison to lipid bilayers, lipid monolayers can be assembled on hydrophobic low-energy surfaces such as photoresists and fluorinated polymers *e.g.* SU8, Teflon AF as monomolecular layers, where the hydrophobic tails of the single layered lipid film are arranged towards the substrate[42]. Although monolayers do not represent plasma membranes very well, as they consist of only half a bilayer and cannot incorporate proteins, they have unique advantages, such as structural simplicity and independence to the buffer composition. Nevertheless, monolayers can still be found in biological systems, such as the lung surfactant, which lowers the surface tension of the alveoli, thus assisting pulmonary compliance[9,10] and the tear film on the corneal epithelium of the eye, which protects it from pathogens and drying[11,12].

It should be noted that on a Teflon-AF surface the edge of the monolayer is diffusive, because Teflon-AF is more hydrophobic than the hydrocarbon chain of the lipids. Therefore it is more favorable for Teflon-AF if the lipids diffuse near the edge. Whereas, the monolayer on SU-8 will yield a more contoured edge as the surface energy of SU-8 is lower than Teflon-AF.

2.4 The Multifunctional Micropipette

The manipulation of fluids in channels with dimensions in the range of micrometers (1-100µm) is called "microfluidics" and it has capabilities which bulk chemistry cannot provide: the ability to handle very small volumes of liquids (10^{-9} to 10^{-18} liters), laminar flow, high resolution and sensitivity in separation and detection, low consumption of samples, solvents and reagents etc.[43]

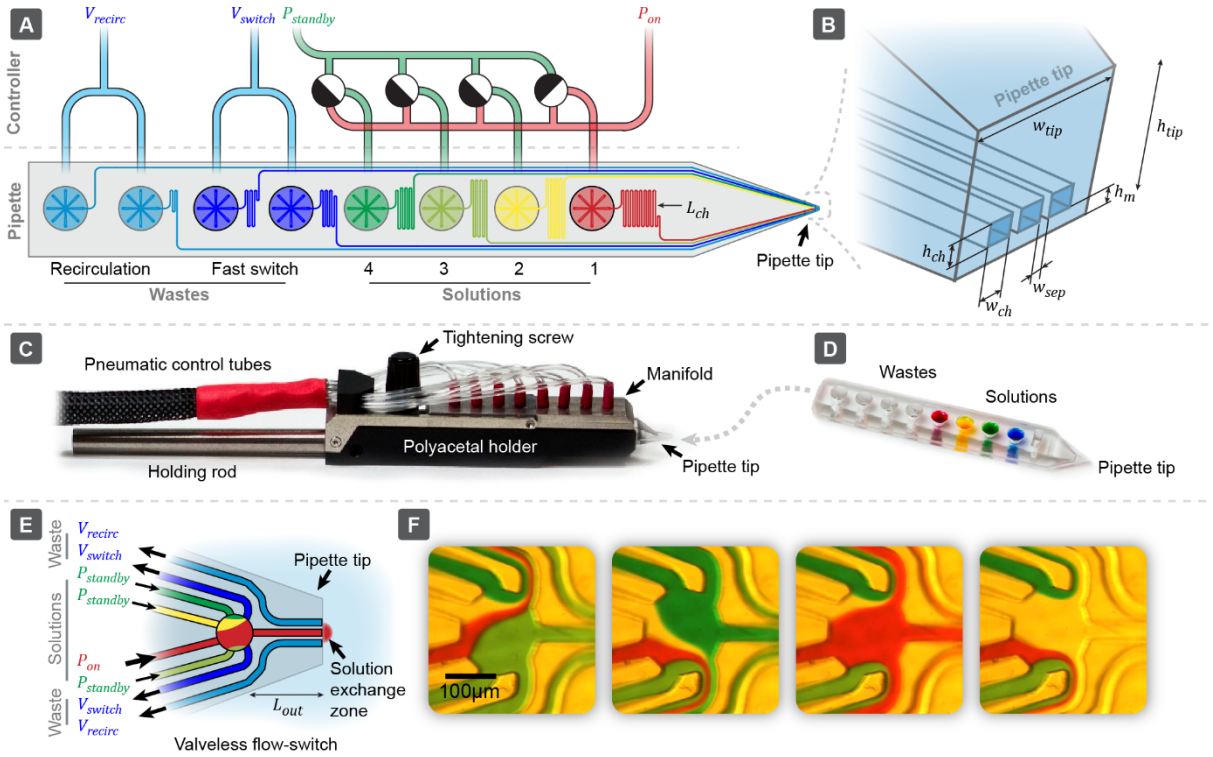

Figure 6 (A) Layout of the on-chip circuitry of the MFP with external connections. The pressures are operated by a pneumatic control unit. (B) Geometries of the pipette tip. (C) The pipette within the holder and (D) separately. (E) Circuitry of the four solution valveless flow-switch. (F) Bright-field microscopy images of different states of the flow-switch, while loaded with different food colors.[44]

The essential component in all of the experiments was the multifunctional micropipette (MFP), which was developed by Ainla *et al*[13]. The MFP is a non-contact open-volume microfluidic device, which utilizes a hydrodynamically confined flow (HFC) at the tip of the pipette to create confined solution environments on surfaces without affecting the surrounding liquid or objects in the vicinity. The pipette has a circuit on the chip and a valveless flow-switch (Figure 6-E), which is controlled by the positive and negative pressures. As the liquid in the small channels exhibits laminar flow, then practically no solution mixing occurs in the flow-switch, which is depicted on Figure 6-F using colored solutions. The confined volume at the tip is maintained by means of positive pressure, injecting a fluid stream out of the tip into an open volume and negative pressures from adjacent channels to aspirate it back into the device,

continuously re-circulating the solution, compensating the diffusion and maintaining a constant concentration.[45–47]

The size of the recirculation zone (solution exchange zone) is controlled by the parameters of the device (Figure 6-A): standby pressure ($P_{standby}$), working pressure (P_{on}), switching vacuum (V_{switch}) and recirculation vacuum (V_{recirc}). The small standby pressure ensures that there is no liquid backflow from one solution well to another. The higher working pressure is applied selectively to the solution well from which solution should be delivered (working solution), while the switching vacuum avoids leakages of other solutions than the working one out of the device. Switching between different pressure levels ("standby" and "on") allows choosing which is the working solution going to be delivered to the surface. The recirculation vacuum and working pressure are used to maintain the HCF and its volume. The pipette features 8 solution reservoirs (wells), of which the first 4 contain lipid suspensions and the last 4 are needed to collect the waste as shown on Figure 6-A. When working pressure is applied to one working solution, it passes through the switching chamber and enters the open volume through the outlet channel. All the other solutions flow through the flow-switch and are routed into the first two fast switch waste wells. The switching time required to change the recirculation volume is <100 ms.

The pipette is fabricated from the optically transparent soft elastomer poly-(dimethylsiloxane) (PDMS) using soft-lithography, which is a relatively simple fabrication method. The measurements of the pipette are shown in Supplementary Table 1 (Appendix 1).

The MFP was used in every experiment as a rapid prototyping tool[15]. The pipette is a multifunctional device which can also be used for delivering drugs in cell cultures and tissue slices[48], single-cell manipulation[44,49] and others without affecting the surrounding liquid.

2.5 Formation techniques of supported membranes

There are multiple techniques to form supported bi- or monolayer membranes, where two traditional methods for the deposition of membranes are Langmuir–Blodgett (LB) and Langmuir-Schaefer (LS)[42,50]. In LB a hydrophilic substrate, such as glass is pulled out from a monolayer-covered air/water interface and an upside-down monolayer is formed. The substrate is thereafter submerged back into the liquid and a bilayer is formed, whereas in LS the substrate is submerged parallel to the surface. The first method can also be used for lipid monolayer deposition, but in this case the glass substrate is hydrophobically modified beforehand[51].

The method used for supported membrane deposition in my research was based on the adsorption and fusion of vesicles using the MFP [15], which utilizes the HFC and as a result overcomes the limitations of the majority of microfluidic platforms, which use closed microchannels for sample analysis.

2.6 Self-spreading of lipid membranes

The spreading of lipids on solid substrates is driven by a surface tension gradient called "Marangoni flow". The driving force of this phenomenon occurs due to the imbalance of forces along the interface and the result is a flow of fluid material from areas of low surface tension towards areas of high surface tension. The spreading of bi- and monolayers are driven by this flow, as the SUVs deposited with the MFP will act as a lipid source. The latter has a low surface tension, whereas the spreading edge has a high surface tension, thus creating a gradient. The driving force for such a flow is the free energy gain in the system per unit area, which is described with the spreading power (S) as:

$$S = \gamma_{Spread} - \gamma_{L-Lipid} = \gamma_{SL} - \gamma_{S-Lipid} - \gamma_{L-Lipid}\,, \qquad 2.6.7$$

where γ_{SL} is the surface tension of the surface wetted with the aqueous buffer, $\gamma_{S-Lipid}$ the surface tension of the substrate wetted with the lipid film and $\gamma_{L-Lipid}$ is the surface tension of the lipid vesicle. For spreading to occur the energy gain γ_{Spread} has to be larger than the surface tension of the lipid vesicle $\gamma_{L-Lipid}$.

Substrate smoothness plays an important role in lipid bilayer spreading. The rougher the substrate, the more bending energy of the lipid bilayer needs to be stored in the system, which is balanced with the energy gain upon bilayer wetting. Moreover, as already elaborated previously in section 2.3.1, buffers can also facilitate lipid bilayer spreading due to multivalent cations.

2.7 Imaging methods

2.7.1 Fluorescence

The majority of the experiments done is this research involved fluorescent microscopy to visualize fluorescent molecules *i.e.* fluorophores attached to lipids and elucidate the processes inside lipid membranes in real-time. For a molecule to fluoresce, certain conditions have to be met, such as high rigidity of the molecule, the presence of electron-donor species, and naturally the molecule has to absorb the excitatory light and favor radiative transitions. When a fluorophore absorbs photons in its excitation wavelength it is excited to a higher quantum state, with a short lifetime, typically in the range of 10^{-7} to 10^{-9} s. The re-emitted photon has a longer wavelength (lower energy) than the absorbed, since a small portion of the absorbed energy is converted into vibrational energy *i.e.* dissipated as heat. The re-emission of light is referred to as fluorescence.

Fluorophores can be conjugated to molecules such as antibodies and lipids, allowing them to be visualized. Importantly, the lipid membranes used in the experiments incorporate a fraction of fluorophore-conjugated lipids, labeled at the hydrophilic head-group of the lipid. Nowadays a large selection of fluorescent dyes, featuring excellent photostability, high fluorescence quantum yield, and a wide range of excitation wavelengths, are available. Introducing several fluorescent dyes with different emission wavelengths gives the possibility to study several molecular species simultaneously.

In the present work, laser light was used to induce fluorescence in the sample to be investigated, coined as the Laser-induced fluorescence (LIF) technique[52] and the diffusivity of the membranes was studied with the fluorescence recovery after photobleaching (FRAP) technique[53].

FRAP is an optical method, which in our case, was used to measure the lateral diffusion in a thin film containing covalently attached fluorescent probes, in our case a fluorophore- labelled lipid membrane. A part of the membrane is exposed to a high-intensity laser beam, which causes photobleaching of the dye - this bleached spot can be seen under the microscope as a dark spot (Figure 7a). Furthermore, if the molecules are able to diffuse, hence the membrane is fluid, then the bleached molecules will mix with the unbleached fluorescent molecules and the darkened area will gradually increase in brightness. The mobile fraction can be calculated from the final intensity after the recovery and the diffusion constant can be calculated from the

recovery time-constant. The calculation is based on fitting to an empirical model derived from computer simulation.

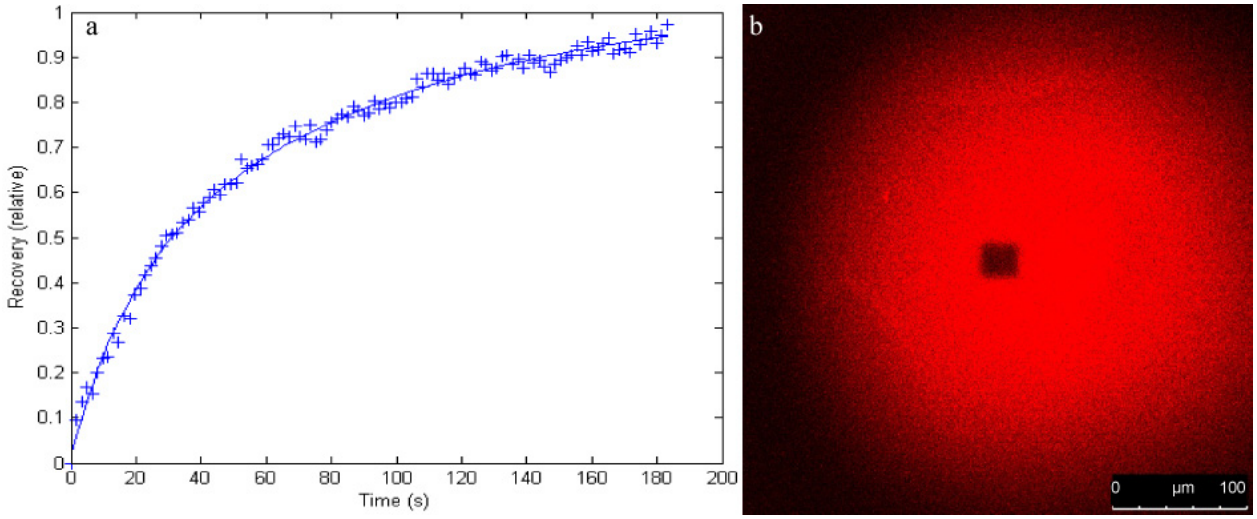

Figure 7 (a) The relative recovery graph (b) and a fluorescent micrograph depicting the bleached region of 50:50 DOTAP:POPC on Teflon-AF.

2.7.2 Confocal laser scanning microscopy

Confocal laser scanning microscopy (CLSM) is a common method of imaging fluorescence[54] in surface-based samples. In a conventional (*i.e.* wide-field) fluorescence microscope, the entire specimen is illuminated evenly and both signals coming from the focal and out of focus plane are collected, whereas confocal microscopes exploit small pinholes, which define a sharp focus point, while illumination intensity and acceptance of light from outside the focal plane are largely blocked by the pinhole. Hence, at any given instant only one point of the sample is observed. During a scan the laser beam is scanned over the sample and the light intensities collected from each point are then reconstructed into an image, one pixel at a time. The focus point can also be scanned vertically *i.e.* in the z-direction and a three-dimensional image of the sample can be constructed in this manner. As a point-source of light is actually an Airy disk, the size of the pinhole must be chosen wisely to match the Airy disk. The more closed the pinhole is, the more light is excluded from the Airy disk, losing useful light. In contrast, the larger the pinhole, the more out-of-focus light is collected to the detector, increasing blur.

CLSM is suitable for surface-based samples, *e.g.* lipid membranes, due to less photobleaching and a better signal-to-noise ratio as laser light back-scattered from the surface is reduced, and was therefore used in this work. In a basic CLSM experiment, the flourophore-labelled lipid

sample is excited by a laser beam at the focal plane. The emission light emanating from the sample is collected through the objective lenses and transferred through the dichroic mirror, which is reflective to one wavelength (shorter) and transmissive to another (longer). The light is thereafter collected through the scanner and pinhole into the detector, which is typically a PMT (photon multiplier tube).

3 Experimental work

3.1 Preparation of small unilamellar vesicles (SUVs)

Lipids with differently charged head groups were used: 1,2-dioleoyl-3-trimethyl-ammoniumpropane (DOTAP) was used as a positive lipid source, 1-palmitoyl-2-oleoyl-*sn*-glycero-3-phosphocholine (POPC) and Soy L-α-phosphatidylcholine (PC) were used as neutral sources and 1,2-dioleoyl-*sn*-glycero-3-phospho-L-serine (DOPS) was chosen for its negatively charged head group. The head-group labelled fluorescent lipids used were ATTO 488 1,2-dioleoyl-*sn*-glycero-3-phosphoethanolamine (ATTO 488-DOPE), ATTO 532 1,2-dioleoyl-*sn*-glycero-3-phosphoethanolamine (ATTO 532-DOPE) and ATTO 655 1,2-dioleoyl-*sn*-glycero-3-phosphoethanolamine (ATTO 655-DOPE) provided by ATTO-TEC GmbH, Germany.

Different lipid mixtures were made with the appropriate fluorescent dyes from chloroform stocks (Avanti polar lipids) to a total concentration of 10 mg/ml. The samples were evaporated in rotary evaporator for 3h at -70kPa to remove the chloroform and thereafter rehydrated overnight in phosphate buffered saline (PBS) (pH 7.8). After rehydration the lipids were diluted with high-ionic strength TRIS buffer (125 mM NaCl (Sigma Aldrich), 10 mM TRIS (VWR), 1 mM Na_2EDTA (Sigma Aldrich), adjusted to pH = 7.4) to a concentration of 1mg/ml and sonicated using a Sonics & Materials Vibra Cell™ High Intensity Ultrasonic Liquid Processor (Model 501, CIAB, Chemical Instruments AB, Sweden) at 15 ^{0}C for 20 minutes (amplitude: 30%) over an ice water bath to make small unilamellar vesicles (SUVs). The solutions were ultracentrifuged (Beckman TL-100 Ultracentrifuge, USA) at 40000 rpm at 15^{0}C for 30 min to separate any larger lipid structures and debris from the mixture. SUV solutions were stored at 4^{0}C until use.

SUVs from different lipid mixtures with about 1% of dye were used to form lipid monolayers on hydrophobic and bilayers on hydrophilic surfaces.

3.2 Surfaces

The Teflon® surfaces were made by spin-coating a layer of Teflon® AF 1600 (poly[4,5-difluoro-2,2-bis(trifluoromethyl)-1,3-dioxole-co-tetrafluoroethylene]) dissolved in pure FC-40 onto circular microscope cover glasses (Menzel-Gläser, 47 mm diameter, obtained from Thermo Scientific, Sweden. They were plasma treated for 2 min (100W) beforehand at 1800 rpm for 1 minute and soft-baked for 30 min at 180 ^{0}C. Some of the Teflon-AF surfaces were

dissolved with perfluoro (2-butyl tetrahydrofuran) (FC-75), which itself was removed with FC-40.

The SU-8 surfaces were made on sonically cleaned cover glasses using the photoresist SU-8 2005 (Microchem Corp., Massachusetts, USA) that was applied via spin-coating at 3000 rpm for 30 s (~5 µm thick), followed by soft baking for 1 min at 95 °C on a hot-plate. The SU-8 film was then flood-exposed with a dose of 6 mJ/cm^2 on a Karl-Süss MA6 i-line (365 nm) mask aligner. Followed by post-baking for 2 min at 95 °C on a hot-plate to finalize the polymerization reaction.

Thin Si_3N_4 films (50 nm thick) were reactive sputtered at 1 kW at $1.3 \cdot 10^{-2}$ mbar with 20 sccm for Ar and 15 sccm for N_2 gas flow rates. 2 nm of Ti adhesion layer (target power - 0.33 kW) and 8 nm of Au (target power - 0.2 kW) were sputtered at $5 \cdot 10^{-3}$ mbar with 40 sccm for Ar gas flow rate. Both films were deposited using FHR-MS 150 sputter system (FHR Anlagenbau GmbH) on pre-cleaned glass covers.

The graphene and SiC samples were obtained from Samuel Lara Avila (Assistant Professor, Microtechnology and Nanoscience, Quantum Device Physics Laboratory, Chalmers University of Technology). A quartz cover square was obtained from SPI® supplies. All of the cover glasses were mounted to a Willco Wells® dish frame using a dedicated double sided tape.

Most steps of fabrication were performed in the cleanroom facility MC2, at Chalmers University of Technology, in the Process Lab 1 with a cleanroom class of 3-6 according to ISO standard 14644-1 (class 1-1000 according to FED-STD-209 E).

3.3 Lipid deposition and imaging

The lipids were deposited using the Multifunctional Pipette™ reported elsewhere[13]. A framed cover glass was filled with PBS buffer (pH=7.8) and the pipette was inserted into the solution. During the experiments, the pipette tip was positioned on the surface for direct material delivery. All experiments were conducted at room temperature.

Fluorescent imaging of the samples was performed using a laser scanning confocal microscope Leica IRE2 (Leica Microsystems GmbH, Wetzlar, Germany) equipped with a Leica TCS SP2 confocal scanner with AOBS™ and Ar/ArKr and HeNe lasers to provide excitation wavelengths at 488, 514 and 633 nm, respectively. A dry HC PL APO CS 20x, numerical

aperture 0.7 objective was used for all confocal experiments. The experimental setup is depicted on Figure 8.

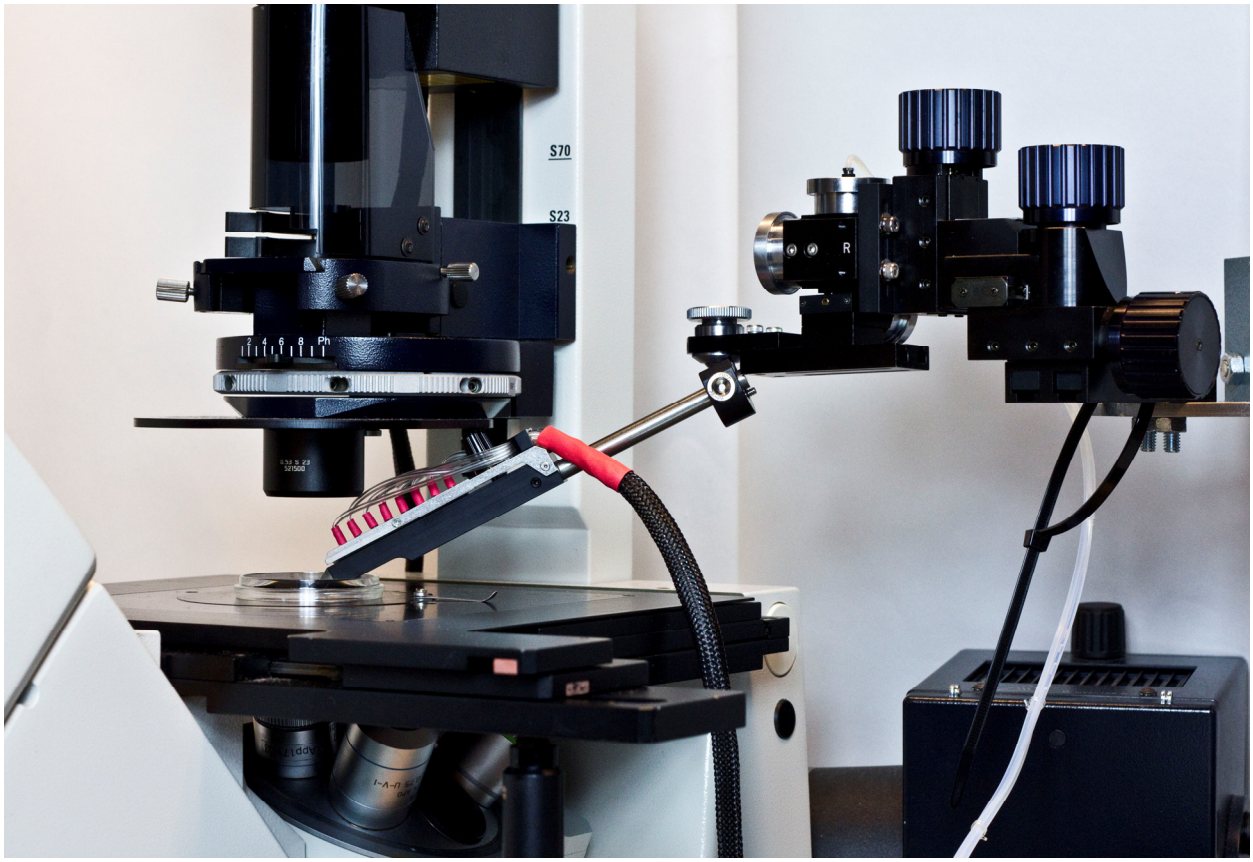

Figure 8 The experimental setup depicting the multifunctional pipette, connected to a micromanipulator in the confocal laser scanning microscope system. The MFP was placed in the corresponding pipette holder and fixed to a micromanipulator for accurate x-y-z movement of the pipette, whereas the sample position was controlled by the stage.

4 Results and discussion

We observed a multitude of behaviors while depositing different lipid mixtures on various surfaces, which are all described in Figure 9. The analysis was separated into two sections according to the hydrophobicity of the surfaces: hydrophilic high-energy surfaces, for potential bilayer formation and hydrophobic low-energy surfaces, where monolayers can be formed. The average spreading velocity, mobile fraction and diffusion coefficients were measured for all experiments.

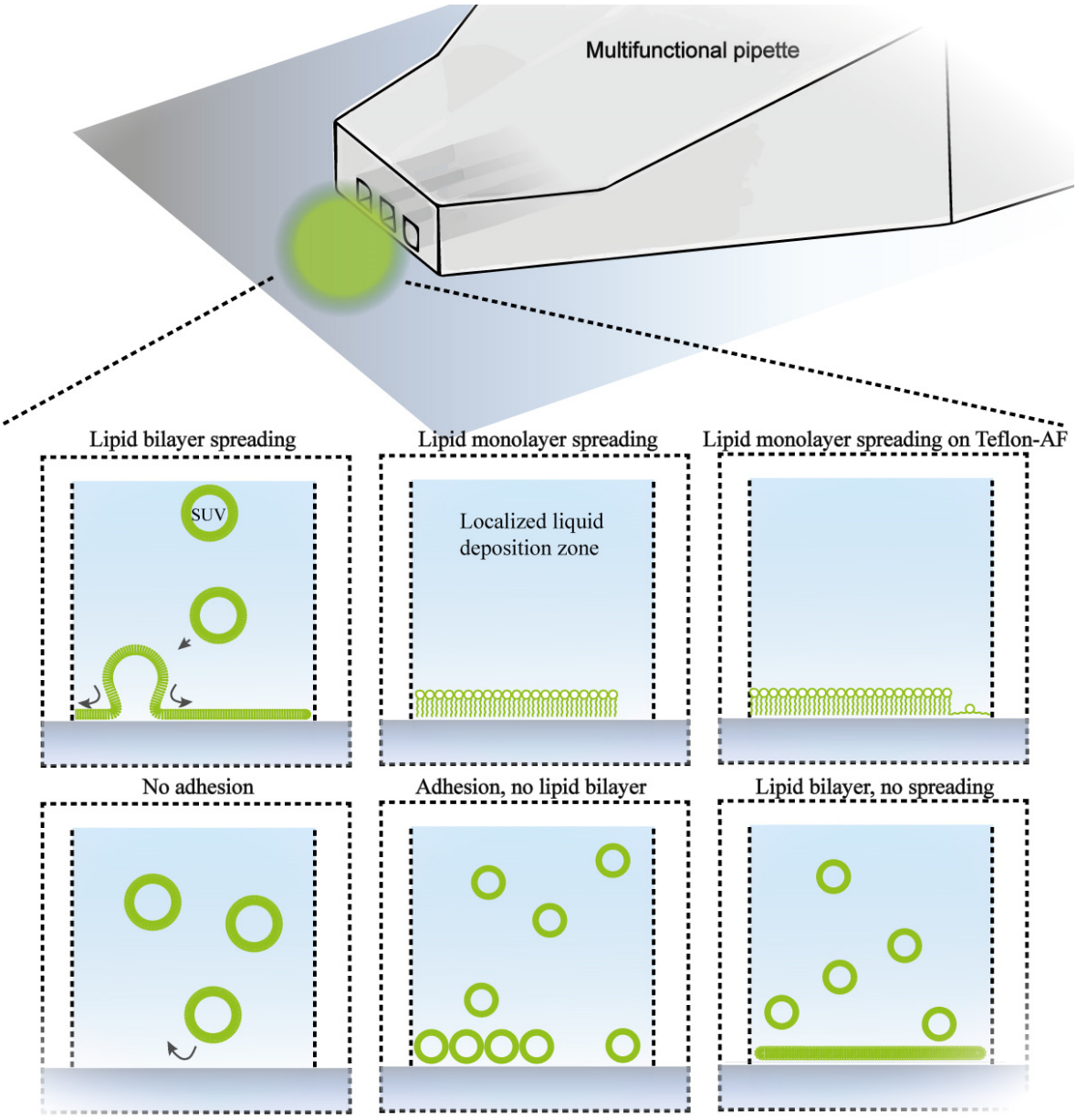

Figure 9 Different lipid behaviors on different surfaces.

4.1 Hydrophilic high-energy surfaces

Several studies on 15 nm thick Au surfaces with various compositions of SUV suspensions were performed and it was seen that no deposition of solutions with any amount of negatively charged head group lipids occurred. The same result was concluded for a neutral suspension which consisted only of a neutral head group lipid POPC. A different situation could be seen while dispensing solutions with moderate amounts of positively charged head-group lipid DOTAP (25%, 50%), where a small amount of deposition was confirmed. After visual inspection it was seen that the lipids formed agglomerates on the surface, which was verified with a subsequent FRAP experiment. However, mixtures with higher amounts of DOTAP did not deposit. It should be noted that roughly 1% of the Au surface is oxidized[55], which is probably the cause why moderately positive suspension forms agglomerates. In order to modify the properties of the Au surface a 5 min 100 W oxygen plasma treatment was made, and an additional experiment showed that the adhesion of positively charged lipid suspension on the surface increased in comparison to the non-treated gold surface. The reason of the increase could lie in the generation of additional hydroxyl groups on the surface, which increases negative charge on the surface and thus allows increased charge interaction with the positively charged head group lipids or the removal of organic surface contaminants with the plasma treatment.

One could presume that similar interactions occur between positive head group lipid suspensions and a negatively charged silicon carbide surface. In order to test this hypothesis a range of lipid suspensions consisting of 25%, 50%, 75% and 99% of DOTAP were used and lipid deposition on the surface could be seen in all cases. To inspect the fluidity of the deposition a FRAP experiment was made, where it could be seen that no fluid membrane was formed. This similarity between Au and SiC is not surprising, due to their intrinsically high surface energies which are in the same order of magnitude, <1000mN/m for Au[56–58] and <2500mN/m for SiC[59].

Borosilicate glass is one of the most widely used substrates for lipid deposition and spreading, which was the reason to test mixtures from 99% negative head group lipids to 99% positive head group lipids. Negative head-group lipids could be deposited on glass, but no membrane fluidity was seen for those cases. Whilst neutral or positive suspensions showed membrane fluidity and the spreading velocity was 0.07 μm/s for 99% POPC and increased with higher amounts of DOTAP in the suspensions – 0.10 μm/s for 25% DOTAP, 0.15 μm/s for 75%, peaking with 0.16 μm/s for 99% DOTAP, which could be expected due to the positive head-

group lipid interactions with the negatively charged glass substrate. From the FRAP experiments full bilayer diffusivity was seen for all SUV compositions. There was a gradual increase in diffusivity from 1.276 $\mu m^2/s$ for 99% POPC to 1.515 $\mu m^2/s$ for 75% DOTAP, whereas the diffusion of 99% DOTAP was the lowest, with a value of 1.24 $\mu m^2/s$.

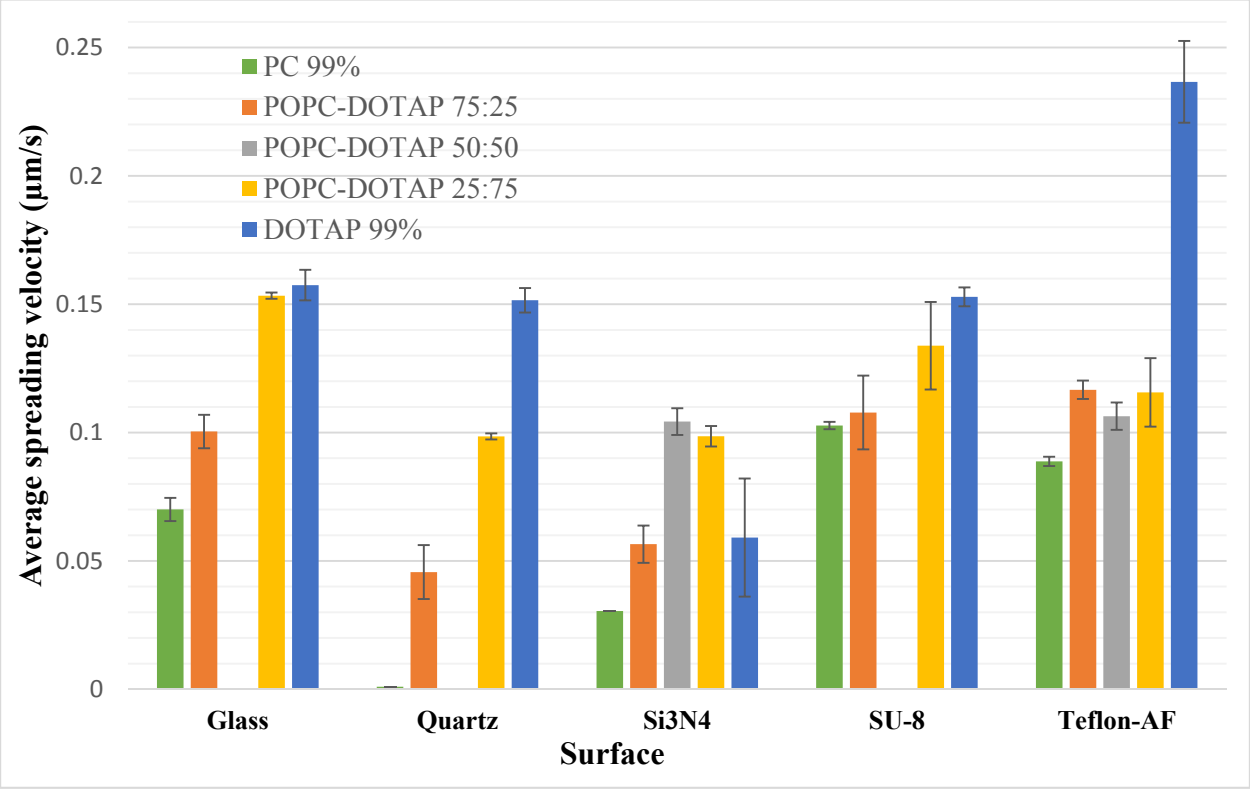

Figure 10 Average spreading velocities on surfaces, where lipid spreading was seen. Error bars are standard deviations on a confidence level of 68%.

Due to the similarity of quartz and glass surfaces, only experiments with different ratios of POPC:DOTAP were dispensed on quartz, omitting the negative head-group lipids. Increasing the amount of positive head-group DOTAP resulted in higher spreading velocities, where a 3-fold increase was seen from 0.05 µm/s to 0.15 µm/s between 25% DOTAP and 99% DOTAP respectively (Figure 10 and Figure 11). For a 99% POPC suspension no spreading was seen and a subsequent FRAP experiment showed no fluid membrane (Table 2). In contrast the diffusion coefficients for suspensions, which contained high amounts of DOTAP (25%, 75% and 99%) had reasonably high values in the magnitude of ~1 $\mu m^2/s$ (the noise was too high to measure a quantitative value) with highly fluid bilayers according to mobile fractions (of ~1).

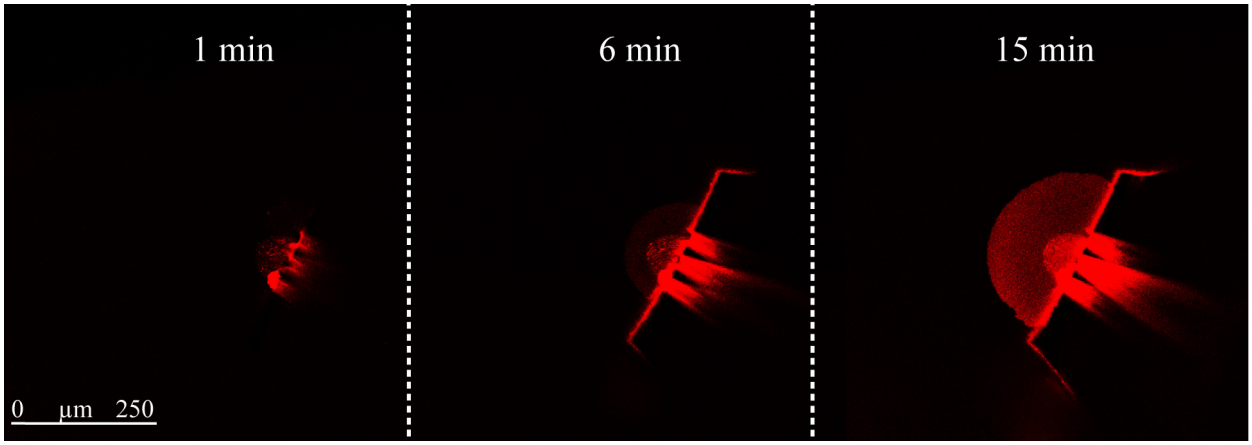

Figure 11 Fluorescence micrographs of 99 % DOTAP spreading as a bilayer on quartz. The snapshots were taken on the times indicated above the respective frames.

In the case of 99% POPC a fluid non-spreading bilayer was seen on glass compared with quartz where no fluidity nor spreading was observed. It could also be inferred that the spreading velocity of 25% DOTAP on glass was twice as high in relation to quartz. However, the 75% DOTAP suspension did not follow this trend, specifically the spreading velocity of 0.10 µm/s on quartz was lower than the corresponding value of 0.15 µm/s on glass. The FRAP data indicated that SUVs deposited on glass had up to 50% higher diffusion coefficients compared with quartz and from all the suspensions in comparison, the only non-fluid deposition was 99% POPC on quartz . On the whole it could be concluded that the spreading velocities were slightly higher on the glass surface, which is reasonable due to the large difference in surface energies between the two surfaces – about 54 mN/m[60] for quartz and <250 mN/m[61,62] for borosilicate glass.

Table 2 Diffusion coefficients (µm^2/s) of various SUVs on different surfaces acquired from FRAP experiments. The blank spaces in the table mean that those experiments were not performed.

Surface	Diffusion coefficient of lipid ($\mu m^2/s$)				
	DOTAP 99%	POPC-DOTAP 25:75	POPC-DOTAP 50:50	POPC-DOTAP 75:25	PC 99%
Glass	1.24(39)	1.515(74)		1.347(51)	1.276(31)
Si_3N_4	1.26(14)	0.932(53)	1.513(44)	0.687(39)	1.59(19)
SU-8	1.67(43)				
Teflon-AF	0.914(73)		1.186(67)		0.00
Dissolved Teflon-AF			0.35(19)		

Several studies on 50 nm thick Si_3N_4 surfaces, the last high-energy surface in question, were made with various compositions of SUV suspensions. All suspensions which contained any amount of negatively charged head-group lipids showed no spreading and were only deposited

as agglomerates. Suspensions with neutral POPC and positive head-group lipid DOTAP were all fully mobile. Compared with quartz, a 99% PC head-group lipid suspension was spreading slightly with an average spreading velocity of 0.03 μm/s on Si_3N_4. The spreading velocity of the POPC:DOTAP 25%:75% mixture on Si_3N_4 was similar to quartz and corresponded to a value of 0.10 μm/s for both cases. This could probably be due to their similar surface energies, which is 51.2 mN/m for Si_3N_4 [60].

While increasing the amount of DOTAP from 25% to 50% a dramatic increase in spreading velocity was seen from 0.06 to 0.10 μm/s, whereas according to Figure 10 there was no significant change in spreading velocity while increasing the amount of DOTAP from 50% to 75% in a suspension. In contrast there was a marked decrease in spreading velocity for a 99% DOTAP mixture, which in relation to spreading on a quartz surface was even twice as low for the same suspension. The latter is probably due to Si_3N_4 surface's isoelectric potential of 9[63], which makes the surface positively charged in the 7.4 pH buffer used in the experiments, and counteracts the spreading of highly positive suspensions. It could be estimated from the FRAP experiments that suspensions with 50% and 99% PC head-group lipids on Si_3N_4 both resulted in the highest diffusion coefficients with values around 1.5 $\mu m^2/s$, which is twice as high as the diffusivity of the 25% DOTAP mixture. The 75% DOTAP suspension, on the other hand, had a moderately high value of 0.93 $\mu m^2/s$. In addition, full bilayer mobility was visible for all cases, as can be seen from the mobile fractions. Although these findings partially support the notion that there is an oxide thin-film on the nitride, the vastly different diffusivities of the POPC suspension on both of the surfaces in this comparison should still be taken into account.

4.2 Hydrophobic low-energy surfaces

As no spreading or deposition was seen for negatively charged head-group lipids on hydrophobic surfaces, then they were excluded from the further analysis.

SUV suspensions containing 25%-75% of DOTAP were dispensed on a graphene surface, which had been grown on SiC (dark lanes on Figure 12), and it could be estimated from a qualitative diffusivity analysis that the 25% DOTAP suspension did not form a fluid membrane. However the fluid 75% DOTAP mixture, suggested at least partial membrane fluidity. Surprisingly, defined spreading along the line of graphene was seen (Figure 12) with a velocity of 0.04 μm/s, while depositing the 50% DOTAP mixture on graphene. Nevertheless the dispensed mixture was largely immobile, adhering to the surface, as could be observed from the recovery (the diffusion coefficient was in the range of ~1 $\mu m^2/s$). This finding confirmed

the notion that, due to graphene's unique properties, it could be used as a lipid sensor, which was also recently shown by Ang *et al* [64] (although they had a bilayer). It should be noted that the FRAP measurements on graphene are only qualitative as it was difficult to visualize the graphene and lipid film at the same time without oversaturating the image.

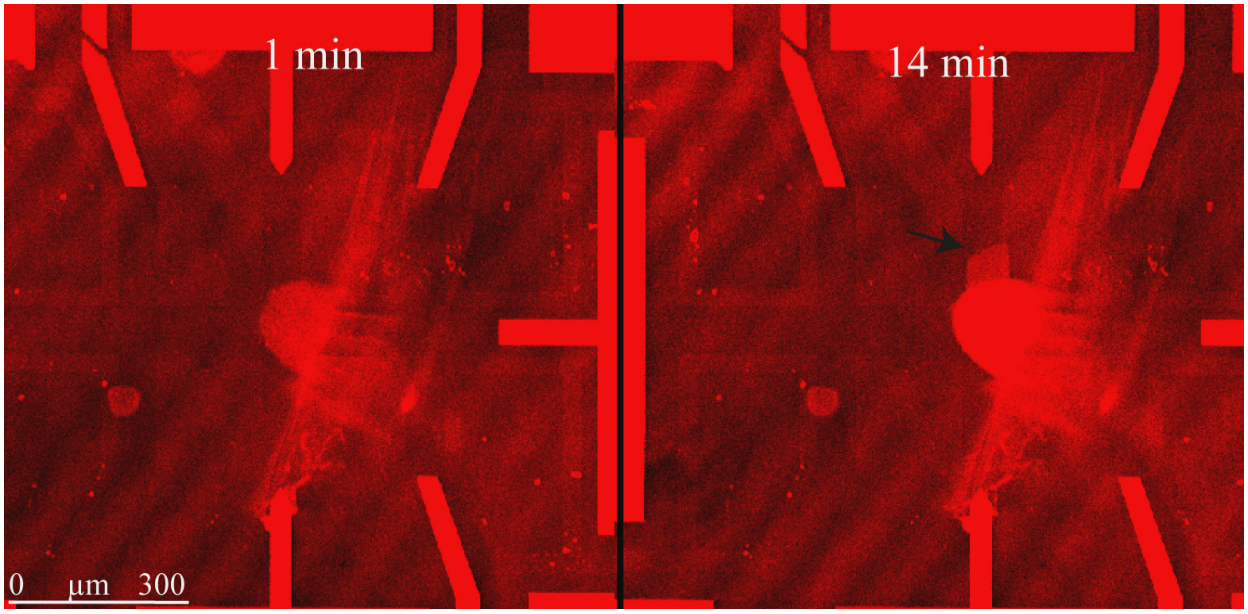

Figure 12 Fluorescence micrographs of POPC-DOTAP 50:50 spreading on a line of graphene. One can see spreading on the frame on the right (depicted with an arrow).

The second lowest energy surface studied was an epoxy resin SU-8, which is used as a negative photoresist, with a surface energy of 47 mN/m[65–67]. Different lipid mixtures consisting of 0%, 25%, 75%, and 99% DOTAP were dispensed on the epoxy surfaces. As can be seen in Figure 10, all of the suspensions tested, had average spreading velocities at least in the 0.1 µm/**s** range and increasing the amount of positive head-group DOTAP, a linear increase in spreading could be seen peaking with a value of 0.15 µm/s for 99% DOTAP, which in relation to 99% PC head-group lipid suspension was 50% higher. A subsequent FRAP experiment made with 99% DOTAP, showed a quite high diffusivity in the range of 1 $\mu m^2/s$ and moderate membrane fluidity with a mobile fraction of 0.7, whereas it could be observed that 99% PC was also a fluid membrane. It should also be noted that the spreading edge of the monolayer on SU-8 has a defined contour (Figure 13).

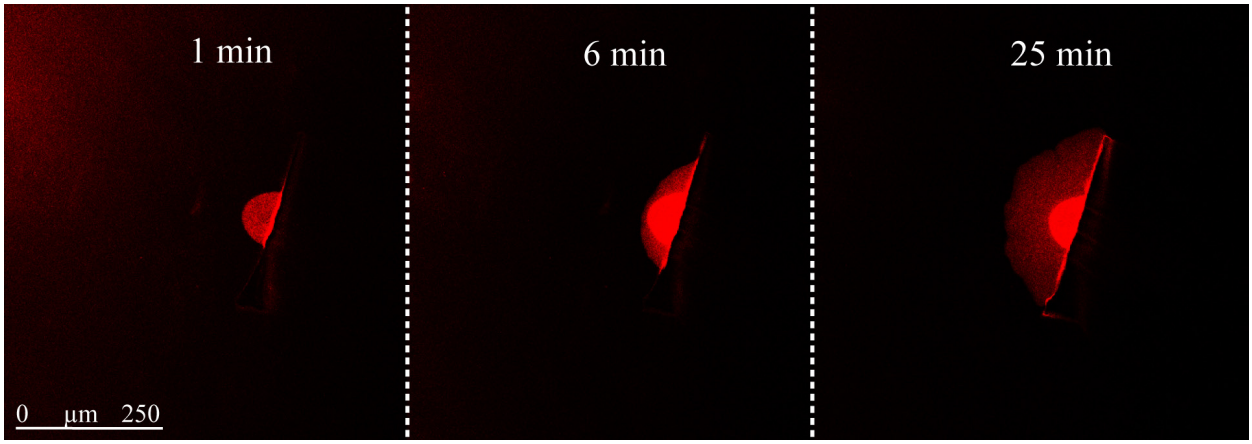

Figure 13 Fluorescence micrographs of Soy PC spreading on SU-8.

It can be estimated from the results that similar spreading processes occurred on Teflon-AF, which is a well-known hydrophobic material. The range of lipids dispensed on the latter, ranged from 99% negative head-group lipid suspensions to 99% positively charged head group lipid DOTAP. At first 99% neutral PC spreading on Teflon-AF could be seen with a spreading velocity of 0.1 µm/s, however this result was not reproduced in several latter experiments where no deposition of PC could be observed and therefore the first experiment will be neglected in the further analysis. The spreading velocity of the 25% DOTAP suspension was 0.12 µm/s as can be estimated from Figure 10, also there was a very minimal decrease in spreading for the 50% DOTAP mixture with a value of 0.11 µm/s. The spreading velocity of 75% DOTAP suspension was again about 0.12 µm/s, similar to the 25% positively charged suspension. In contrast a marked rise in spreading of the 99% highly positive DOTAP mixture was seen (Figure 14), with a spreading value of ~0.24 µm/s, which being the highest value of all the experiments, is twice as high as the 75% DOTAP suspension's. This favorable spreading can be explained with the direct charge interaction between the positive head-groups of the lipid and negatively charged Teflon-AF surface, in addition to the low energy (>14 mN/m[68]) of the surface. From the FRAP experiments for the 50% and 99% DOTAP suspensions, full monolayer diffusivity was seen with diffusion coefficients of 1.2 and 0.9 $\mu m^2/s$, respectively.

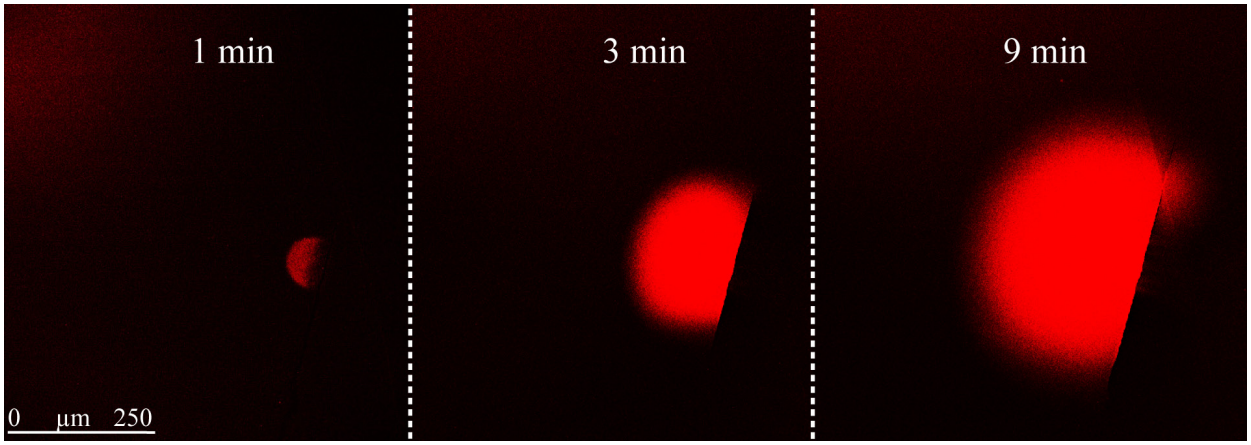

Figure 14 Fluorescence micrographs of 99% DOTAP spreading on Teflon-AF. A diffuse edge of spreading is seen for the case of Teflon-AF.

A subsequent experiment with a 50% DOTAP mixture on a partially dissolved Teflon-AF surface was made, in order to alter the properties of the substrate. A comparatively similar lipid film diffusivity was seen with slightly different spreading properties – a marked increase in spreading of the suspension on dissolved Teflon-AF was concluded (value of 0.16 $\mu m^2/s$). The increased spreading could be explained with the decrease in the surface roughness of the porous Teflon-AF, which is known to alter lipid spreading[25]. The lipid film remained fully mobile, even though the diffusion of the lipid on the unmodified surface was nearly three times as high in relation to the modified surface.

The analysis of both surface types led to some general behaviors of lipid membranes on different surfaces, as hypothesized and therefore affirmed the validity of the extendibility of the lab on a biomembrane technique to a multitude of different environments.

5 Conclusion

In this work we report the expansion of the novel lab on a biomembrane technique, which was used on a multitude of support materials, as a practical and versatile approach to facilitate membrane studies and to initiate lipid spreading on those surfaces.

In the first section of the work the theory behind fabrication methods and research techniques such as surfaces properties, supported lipid membranes, confocal fluorescence microscopy and the multifunctional pipette, were covered. The experimental part elaborated the preparation of the SUV-s and different surfaces for lipid deposition and imaging with the multifunctional pipette in the confocal fluorescence microscope system. In the second part of the thesis, the spreading and deposition properties of supported lipid membranes were studied on the corresponding surfaces and analyzed accordingly.

I have collected data of 9 different compositions of lipid suspensions on 8 different high– and low-energy surfaces. Depending on the lipid composition, adhesion or membrane formation could be achieved on almost all investigated surfaces. Different lipid species were combined, such as DOTAP and POPC to find out the optimal compositions for the corresponding surfaces. The positive transfection lipid DOTAP facilitated spreading, which was consistent for nearly all surfaces. One of the most important results were that lipid monolayer spreading could be observed on graphene, while depositing the 50:50 DOTAP:POPC suspension. Due to the unique properties of graphene, it could be used as a lipid sensor for future sensing applications. No spreading occurred on gold, even after high-energy plasma treatments, although some deposition was affirmed, due to the generation of additional hydroxyl groups. Two different monolayer spreading mechanisms were seen – diffusive and contoured. The highest spreading velocity was achieved on Teflon-AF. In conclusion, through the right choice of the lipid mixture one can initiate formation of fluid lipid films on practically all surfaces.

In the future this method could be used as a powerful tool in designing various nanofluidic analytical systems, reactors and sensors, which could open new venues for studying biomolecular interactions in membranes such as the molecular mechanisms of membrane attached protein receptor complexes involved in various cell signaling processes or exocytosis in the chemical synapse, and most importantly this system could be efficiently used to optimize lipid membranes for biosensor applications.

6 Acknowledgements

This research was supported by national scholarship program Kristjan Jaak, which is funded and managed by Archimedes Foundation in collaboration with the Ministry of Education and Research.

I would like to thank Anna-Liisa and Alar for proof-reading my thesis and Regina for her help on language-related questions.

I am most grateful to my supervisor Alar and Aldo for letting me do the experiments in the Biophysical Technology lab at Chalmers University of Technology and help me master all the required apparatus with the additional help from Gavin, Tanya and Kiryl. All the other members of the Biophysical Technology lab whom I made contact with will also receive a thank you for creating a fun and enjoyable workplace! I especially appreciate that Alar, who moved to Harvard University during my stay in Gothenburg, still found the time to supervise and support me via Skype despite the long distance between us. But let us not forget the warm and supportive environment in the Intelligent Materials and Systems lab, especially my Estonian supervisor Alvo, who has given me invaluable advice not only on science-related questions but even more generally.

The contribution of Alar, Aldo and Tanya to help me write the article's manuscript (and arrange my thoughts), which will be published soon, was also noteworthy.

Sooviksin tänada ka oma sõpru, keda ma väärtustan väga, kuid ei pruugi seda alati välja näidata ning oma abivalmis ja heasüdamlikku ema.

7 Lipiidmembraanide ja tahkete pindade omavaheliste interaktsioonide karakteriseerimine, kasutades multifunktsionaalset pipetti

Silver Jõemetsa

Rakku ümbritseb suuresti fosfolipiididest koosnev membraan, mille funktsioonide ja ehituslike omaduste paremini mõistmine on ülioluline: membraan eraldab raku sisest – ja välist keskkonda, olles ka selektiivne poolläbilaskev membraan, mis võimaldab erinevaid transpordimehhanisme, näiteks rakumembraanis olevate proteiinide vahendusel toimub aktsioonipotentsiaali edasikandumine närvirakkudes.

Käesolev töö käsitleb uudse *Lab on a Biomembrane* (LoaBM) meetodi edasiarendamist, mis hõlbustab rakumembraanide ja selle komponentide omaduste ja omavaheliste interaktsioonide uurimist, leides rakendust näiteks ravimitööstuses, tehisraku biofüüsikalise mudeli edasiarendamisel, muu hulgas ka neuraalsete haiguste ja vähi edasileviku mehhanismi uurimisel. Antud meetodit kasutati erinevatel alusmaterjalidel kui lihtsat ja praktilist tööriista lipiidide pindadele kandmiseks. Teostati süstemaatiline uuring multifunktsionaalse pipeti abil, uurimaks lipiidsegu koostise ja pinna omaduste mõju lipiidide laialivalgumisele ja pinnale kandmisele.

Töö esimeses pooles käsitleti teoreetiliselt erinevaid fabritseerimismeetodeid, pinna omadusi, toestatud lipiidmembraane, konfokaal-fluorestsentsmikroskoopi ja multifunktsionaalset pipetti. Eksperimentaalses osas kirjeldati, kuidas valmistati ette erinevaid pindasid ja ühekihilisi lipiidvesiikuleid (SUV), mida hiljem multifunktsionaalse pipetiga pinnale kanti ja konfokaal-fluorestsentsmikroskoobi süsteemis visualiseeriti.

Töö teises pooles uuriti toestatud lipiidmembraanide pindadele kandmise ja laialivalgumise omadusi erinevatel aluspindadel.

Uuriti kaheksat erinevat kõrge- ja madala energiaga pinda (Au, borosilikaat-klaas, kvarts, Si_3N_4, SiC, SU-8, grafeen ja Teflon-AF), sealjuures üheksa erineva kontsentratsiooniga lipiidsuspensiooni, mis sisaldasid erinevates vahekordades anioonseid ja katioonseid lipiide: DOTAP, POPC, Soja PC ja DOPS koos väikse hulga fluorofooriga seotud lipiide. Leiti optimaalsed kontsentratsioonid laialivalgumise saavutamiseks eri pindadel. Positiivse peagrupiga lipiid DOTAP hõlbustas laialivalgumist enamikel pindadel. Üks olulisematest tulemustest oli lipiidmonokihi laialivalgumine grafeeni pinnal, mis saavutati 50:50 DOTAP:POPC suspensiooniga. Grafeeni unikaalsete omaduste tõttu võiks seda kasutada

tulevikus lipiidsensorina. Kulla peal see-eest laialivalgumist ei nähtud, isegi peale plasmatöötlust, kuid osaline depositeerimine oli võimalik tänu täiendavate hüdroksüülrühmade moodustumisele pinnal. Eristati kahte monokihi laialivalgumise viisi: difuusne ja kontuuriga, ning suurim laialivalgumise kiirus saavutati Teflon-AF pinnal. Kokkuvõtteks on võimalik moodustada lipiidkile praktiliselt igal pinnal, kasutades õige kontsentratsioonide vahekorraga lipiidsegu.

Need katsed demonstreerivad LoaBM meetodi universaalset rakendatavust. Seda saaks kasutada erinevate nanovedelik-analüütiliste süsteemide, reaktorite ja sensorite kujundamiseks, mis omakorda aitaksid uurida membraanides olevaid biomolekulaarseid interaktsioone, nagu eksotsütoos keemilises sünapsis.

27.05.2015

8 References

(1) Alberts, B.; Johnson, A.; Lewis, J.; Raff, M.; Roberts, K.; Walter, P. *MOLECULAR BIOLOGY OF THE CELL, 5TH EDITION*; 2007; Vol. 4, p 1392.

(2) Sackmann, E. Supported Membranes: Scientific and Practical Applications. *Science (80-.).* **1996**, *271* (5245), 43–48.

(3) Plant, A. L. Supported Hybrid Bilayer Membranes as Rugged Cell Membrane Mimics. *Langmuir* **1999**, *15* (15), 5128–5135.

(4) Nissen, J.; Gritsch, S.; Wiegand, G.; Rädler, J. O. Wetting of Phospholipid Membranes on Hydrophilic Surfaces - Concepts towards Self-Healing Membranes. *Eur. Phys. J. B* **1999**, *10* (2), 335–344.

(5) Sanii, B.; Parikh, A. N. Surface-Energy Dependent Spreading of Lipid Monolayers and Bilayers. *Soft Matter* **2007**, *3* (8), 974.

(6) Czolkos, I.; Erkan, Y.; Dommersnes, P.; Jesorka, A.; Orwar, O. Controlled Formation and Mixing of Two-Dimensional Fluids. *Nano Lett.* **2007**, *7* (7), 1980–1984.

(7) Richter, R.; Bérat, R.; Brisson, A. Formation of Solid-Supported Lipid Bilayers: An Integrated View. *Langmuir* **2006**, No. 12, 3497–3505.

(8) Egrot, A. P. G.; Marquette, C. A.; Blum, L. J. Biomimetic Membranes and Biomolecule Immobilisation Strategies for Nanobiotechnology Applications. *Int. J. Nanotechnol.* **2010**, *7* (4/5/6/7/8), 753.

(9) Ding, J.; Takamoto, D. Y.; von Nahmen, a; Lipp, M. M.; Lee, K. Y.; Waring, a J.; Zasadzinski, J. a. Effects of Lung Surfactant Proteins, SP-B and SP-C, and Palmitic Acid on Monolayer Stability. *Biophys. J.* **2001**, *80* (5), 2262–2272.

(10) Baoukina, S.; Tieleman, D. P. Lung Surfactant Protein SP-B Promotes Formation of Bilayer Reservoirs from Monolayer and Lipid Transfer between the Interface and Subphase. *Biophys. J.* **2011**, *100* (7), 1678–1687.

(11) Bron, a. J.; Tiffany, J. M.; Gouveia, S. M.; Yokoi, N.; Voon, L. W. Functional Aspects of the Tear Film Lipid Layer. *Exp. Eye Res.* **2004**, *78* (3), 347–360.

(12) Kulovesi, P.; Telenius, J.; Koivuniemi, A.; Brezesinski, G.; Rantamäki, A.; Viitala, T.; Puukilainen, E.; Ritala, M.; Wiedmer, S. K.; Vattulainen, I.; Holopainen, J. M. Molecular Organization of the Tear Fluid Lipid Layer. *Biophys. J.* **2010**, *99* (8), 2559–2567.

(13) Ainla, A.; Jeffries, G. D. M.; Brune, R.; Orwar, O.; Jesorka, A. A Multifunctional Pipette. *Lab Chip* **2012**, *12* (7), 1255–1261.

(14) Zagnoni, M. Miniaturised Technologies for the Development of Artificial Lipid Bilayer Systems. *Lab Chip* **2012**, *12* (6), 1026–1039.

(15) Ainla, A.; Gözen, I.; Hakonen, B.; Jesorka, A. Lab on a Biomembrane: Rapid Prototyping and Manipulation of 2D Fluidic Lipid Bilayers Circuits. *Sci. Rep.* **2013**, *3*, 2743.

(16) Adhikari, C.; Das, A.; Chakraborty, A. Controlled Release of a Sparingly Water-Soluble Anticancer Drug through pH-Responsive Functionalized Gold-Nanoparticle-Decorated Liposomes. *Chemphyschem* **2015**, *16* (4), 866–871.

(17) Shuttleworth, R. The Surface Tension of Solids. *Proc. Phys. Soc. Sect. A* **1950**, *63* (5), 444–457.

(18) Jolivet, J.-P.; Henry, M.; Livage, J.; Bescher, E. *Metal Oxide Chemistry and Synthesis: From Solution to Solid State*; John Wiley New York, 2000; p 338.

(19) De Gennes, P. Wetting: Statics and Dynamics. *Rev. Mod. Phys.* **1985**, *57* (3), 827–863.

(20) Nychka, J. A.; Gentleman, M. M. Implications of Wettability in Biological Materials Science. *JOM* **2010**, *62* (7), 39–48.

(21) Giovambattista, N.; Debenedetti, P. G.; Rossky, P. J. Effect of Surface Polarity on Water Contact Angle and Interfacial Hydration Structure. *J. Phys. Chem. B* **2007**, *111* (32), 9581–9587.

(22) Wenzel, R. N. RESISTANCE OF SOLID SURFACES TO WETTING BY WATER. *Ind. Eng. Chem.* **1936**, *28* (8), 988–994.

(23) Gao, X.; Jiang, L. Biophysics: Water-Repellent Legs of Water Striders. *Nature* **2004**, *432* (7013), 36.

(24) Cassie, A.; Baxter, S. Wettability of Porous Surfaces. *Trans. Faraday Soc.* **1944**, No. 5, 546–551.

(25) Dorrer, C.; Rühe, J. Some Thoughts on Superhydrophobic Wetting. *Soft Matter* **2009**, *5* (1), 51.

(26) Nosonovsky, M.; Bhushan, B. Biologically Inspired Surfaces: Broadening the Scope of Roughness**. *Adv. Funct. Mater.* **2008**, *18* (6), 843–855.

(27) Marmur, A. Wetting on Hydrophobic Rough Surfaces: To Be Heterogeneous or Not To Be? *Langmuir* **2003**, *19* (20), 8343–8348.

(28) Emslie, A. G.; Bonner, F. T.; Peck, L. G. Flow of a Viscous Liquid on a Rotating Disk. *J. Appl. Phys.* **1958**, *29* (5), 858.

(29) Fahy, E.; Subramaniam, S.; Brown, H. A.; Glass, C. K.; Merrill, A. H.; Murphy, R. C.; Raetz, C. R. H.; Russell, D. W.; Seyama, Y.; Shaw, W.; Shimizu, T.; Spener, F.; van Meer, G.; VanNieuwenhze, M. S.; White, S. H.; Witztum, J. L.; Dennis, E. a. A Comprehensive Classification System for Lipids. *J. Lipid Res.* **2005**, *46* (5), 839–861.

(30) Jacob, N.; Israelachvili, N. Intermolecular and Surface Forces. *San Diego Acad.* **1992**.

(31) Breslow, R. Hydrophobic Effects on Simple Organic Reactions in Water. *Acc. Chem. Res.* **1991**, *24* (6), 159–164.

(32) Chan, Y.-H. M.; Boxer, S. G. Model Membrane Systems and Their Applications. *Curr. Opin. Chem. Biol.* **2007**, *11* (6), 581–587.

(33) Jones, R. A. L. *Soft Condensed Matter*; Oxford University Press, 2003; p 202.

(34) Gözen, I.; Jesorka, A. Instrumental Methods to Characterize Molecular Phospholipid Films on Solid Supports. *Anal. Chem.* **2012**, *84* (2), 822–838.

(35) Rädler, J.; Strey, H.; Sackmann, E. Phenomenology and Kinetics of Lipid Bilayer Spreading on Hydrophilic Surfaces. *Langmuir* **1995**, No. 8, 4539–4548.

(36) Israelachvili, J. N.; Marcelja, S.; Horn, R. G. Physical Principles of Membrane Organization. *Q. Rev. Biophys.* **1980**, *13* (2), 121–200.

(37) Tamm, L. K.; McConnell, H. M. Supported Phospholipid Bilayers. *Biophys. J.* **1985**, *47* (1), 105–113.

(38) Johnson, S. J.; Bayerl, T. M.; McDermott, D. C.; Adam, G. W.; Rennie, a R.; Thomas, R. K.; Sackmann, E. Structure of an Adsorbed Dimyristoylphosphatidylcholine Bilayer Measured with Specular Reflection of Neutrons. *Biophys. J.* **1991**, *59* (2), 289–294.

(39) Castellana, E. T.; Cremer, P. S. Solid Supported Lipid Bilayers: From Biophysical Studies to Sensor Design. *Surf. Sci. Rep.* **2006**, *61* (10), 429–444.

(40) Reboiras, M. D. Activity Coefficients of CaCl 2 and MgCl 2 in the Presence of Dipalmitoylphosphatidylcholine-Phosphatidylinositol Vesicles in Aqueous Media. *Bioelectrochemistry Bioenerg.* **1996**, *39* (1), 101–108.

(41) Lobovkina, T.; Gözen, I.; Erkan, Y.; Olofsson, J.; Weber, S. G.; Orwar, O. Protrusive Growth and Periodic Contractile Motion in Surface-Adhered Vesicles Induced by Ca2+-Gradients. *Soft Matter* **2010**, *6* (2), 268–272.

(42) Czolkos, I.; Jesorka, A.; Orwar, O. Molecular Phospholipid Films on Solid Supports. *Soft Matter* **2011**, *7* (10), 4562.

(43) Whitesides, G. M. The Origins and the Future of Microfluidics. *Nature* **2006**, *442* (7101), 368–373.

(44) Xu, S.; Ainla, A.; Jardemark, K.; Jesorka, A.; Jeffries, G. D. M. A Heating-Superfusion Platform Technology for the Investigation of Protein Function in Single Cells. *Anal. Chem.* **2015**, *87* (1), 381–387.

(45) Juncker, D.; Schmid, H.; Delamarche, E. Multipurpose Microfluidic Probe. *Nat. Mater.* **2005**, *4* (8), 622–628.

(46) Ainla, A.; Jansson, E. T.; Stepanyants, N.; Orwar, O.; Jesorka, A. A Microfluidic Pipette for Single-Cell Pharmacology. *Anal. Chem.* **2010**, *82* (11), 4529–4536.

(47) Christ, K. V; Turner, K. T. Design of Hydrodynamically Confined Microfluidics: Controlling Flow Envelope and Pressure. *Lab Chip* **2011**, *11* (8), 1491–1501.

(48) Ahemaiti, A.; Wigström, H.; Ainla, A.; Jeffries, G. D. M.; Orwar, O.; Jesorka, A.; Jardemark, K. Spatial Characterization of a Multifunctional Pipette for Drug Delivery in Hippocampal Brain Slices. *J. Neurosci. Methods* **2015**, *241*, 132–136.

(49) Xu, S.; Kim, A.; Jeffries, G. D. M.; Jesorka, A. A Rapid Microfluidic Technique for Integrated Viability Determination of Adherent Single Cells. *Anal. Bioanal. Chem.* **2015**, *407* (5), 1295–1301.

(50) Charitat, T.; Bellet-Amalric, E.; Fragneto, G.; Graner, F. Adsorbed and Free Lipid Bilayers at the Solid-Liquid Interface. *Eur. Phys. J. B* **1999**, *8* (4), 583–593.

(51) Tscharner, V. von; McConnell, H. An Alternative View of Phospholipid Phase Behavior at the Air-Water Interface. Microscope and Film Balance Studies. *Biophys. J.* **1981**, *36* (November), 409–419.

(52) Kinsey, J. L. Laser-Induced Fluorescence. *Annu. Rev. Phys. Chem.* **1977**, *28* (1), 349–372.

(53) Peters, R.; Peters, J.; Tews, K. H.; Bähr, W. A Microfluorimetric Study of Translational Diffusion in Erythrocyte Membranes. *Biochim. Biophys. Acta - Biomembr.* **1974**, *367* (3), 282–294.

(54) Minsky, M. Microscopy Apparatus, 1961.

(55) Wipf, M.; Stoop, R. L.; Tarasov, A.; Bedner, K.; Fu, W.; Wright, I. A.; Martin, C. J.; Constable, E. C.; Calame, M.; Schönenberger, C. Selective Sodium Sensing with Gold-Coated Silicon Nanowire Field-Effect Transistors in a Differential Setup. *ACS Nano* **2013**, *7* (7), 5978–5983.

(56) Needs, R.; Mansfield, M. Calculations of the Surface Stress Tensor and Surface Energy of the (111) Surfaces of Iridium, Platinum and Gold. *J. Phys. Condens. Matter* **1989**, *7555*.

(57) Crljen, Ž.; Lazić, P.; Šokčević, D.; Brako, R. Relaxation and Reconstruction on (111) Surfaces of Au, Pt, and Cu. *Phys. Rev. B* **2003**, *68* (19), 195411.

(58) Corti, C.; Holliday, R. *Gold: Science and Applications*; Taylor & Francis Group, 2009; p 444.

(59) Maximenko, S.; Pirouz, P.; Sudarshan, T. Open Core Dislocations and Surface Energy of SiC. *Mater. Sci. forum* **2006**, *529*, 439–442.

(60) Pignataro, B.; Grasso, G.; Renna, L.; Marletta, G. Adhesion Properties on Nanometric Scale of Silicon Oxide and Silicon Nitride Surfaces Modified by 1-Octadecene. *Surf. Interface Anal.* **2002**, *33* (2), 54–58.

(61) Tillotson, E. W. On the Surface Tension of Silicate and Borosilicate Glasses. *J. Ind. Eng. Chem.* **1912**, *4* (9), 651–652.

(62) Rhee, S. Surface Energies of Silicate Glasses Calculated from Their Wettability Data. *J. Mater. Sci.* **1977**, *12*, 823–824.

(63) Lewis, J. A. Colloidal Processing of Ceramics. **2000**, *59*, 2341–2359.

(64) Ang, P. K.; Jaiswal, M.; Haley, C.; Xuan, Y.; Wang, Y.; Sankaran, J.; Loh, K. P.; Li, A.; Lim, C. T.; Wohland, T. A Bioelectronic Platform Using a Graphene− Lipid Bilayer Interface. *ACS Nano* **2010**, *4* (12), 7387–7394.

(65) Zhang, J.; Zhou, W. X.; Chan-Park, M. B.; Conner, S. R. Argon Plasma Modification of SU-8 for Very High Aspect Ratio and Dense Copper Electroforming. *J. Electrochem. Soc.* **2005**, *152* (10), C716.

(66) Fakhfouri, V.; Mermoud, G.; Kim, J.; Martinoli, A.; Brugger, J. Drop-On-Demand Inkjet Printing of SU-8 Polymer. *Micro Nanosyst.* **2009**, *1* (1), 63–67.

(67) Czolkos, I. *Micro- and Nano-Scale Devices for Controlling Two-Dimensional Chemistry*; Department of Chemical and Biological Engineering, Physical Chemistry, Chalmers University of Technology: Göteborg, 2009.

(68) Drummond, C. J.; Georgaklis, G.; Chan, D. Y. C. Fluorocarbons: Surface Free Energies and van Der Waals Interaction. *Langmuir* **1996**, *12* (11), 2617–2621.

Appendix 1.

Supplementary Table 1 The measurements of the MFP.

Description	**Symbol**	**Value**	**Unit**
Length of main channels	L_{ch}	62	mm
Length of outlet channel	L_{out}	300	µm
Width of channels	w_{ch}	27.90 (90)	µm
Height of channels	h_{ch}	35.5 (13)	µm
Separation of channels at the tip	w_{sep}	18.29 (69)	µm
Thickness of the bottom membrane	w_{sep}	19.66 (61)	µm
Total width of the tip	w_{tip}	309 (51)	µm
Height of the tip	h_{tip}	1	mm
Volume of reservoirs	V_{res}	35	µL

Lihtlitsents lõputöö reprodutseerimiseks ja lõputöö üldsusele kättesaadavaks tegemiseks

Mina, Silver Jõemetsa

(sünnikuupäev: 27.11.1990)

1. annan Tartu Ülikoolile tasuta loa (lihtlitsentsi) enda loodud teose:

RAPID PROTOTYPING AND CHARACTERIZATION OF LIPID MEMBRANES ON SOLID SURFACES,

mille juhendaja on Alvo Aabloo, Alar Ainla ja Aldo Jesorka,

1.1. reprodutseerimiseks säilitamise ja üldsusele kättesaadavaks tegemise eesmärgil, sealhulgas digitaalarhiivi DSpace-is lisamise eesmärgil kuni autoriõiguse kehtivuse tähtaja lõppemiseni;

1.2. üldsusele kättesaadavaks tegemiseks Tartu Ülikooli veebikeskkonna kaudu, sealhulgas digitaalarhiivi DSpace´i kaudu alates **25.05.2016** kuni autoriõiguse kehtivuse tähtaja lõppemiseni.

2. olen teadlik, et nimetatud õigused jäävad alles ka autorile.

3. kinnitan, et lihtlitsentsi andmisega ei rikuta teiste isikute intellektuaalomandi ega isikuandmete kaitse seadusest tulenevaid õigusi.

Tartus **27.05.2015**